AGU PUBLICATIONS

Geochemistry, Geophysics, Geosystems

RESEARCH ARTICLE
10.1002/2015GC006218

Key Points:
- Fish tooth Nd isotopic composition is not affected by changing pore water redox conditions
- Consistently positive fish tooth Ce anomaly not driven by pore water redox conditions
- Organic coatings on fossil fish teeth contain up to 70% of the total REEs

Supporting Information:
- Supporting Information S1
- Table S1

Correspondence to:
C. E. Huck,
c.e.huck@soton.ac.uk

Citation:
Huck, C. E., T. van de Flierdt, F. J. Jiménez-Espejo, S. M. Bohaty, U. Röhl, and S. J. Hammond (2016), Robustness of fossil fish teeth for seawater neodymium isotope reconstructions under variable redox conditions in an ancient shallow marine setting, *Geochem. Geophys. Geosyst.*, *17*, 679–698, doi:10.1002/2015GC006218.

Received 4 DEC 2015
Accepted 5 FEB 2016
Accepted article online 12 FEB 2016
Published online 7 MAR 2016

Robustness of fossil fish teeth for seawater neodymium isotope reconstructions under variable redox conditions in an ancient shallow marine setting

Claire E. Huck[1,2], Tina van de Flierdt[1], Francisco J. Jiménez-Espejo[3], Steven M. Bohaty[2], Ursula Röhl[4], and Samantha J. Hammond[5]

[1]Department of Earth Science and Engineering, Imperial College London, London, UK, [2]Department of Ocean and Earth Science, University of Southampton, National Oceanography Centre, Southampton, UK, [3]Department of Biogeochemistry, Japan Agency for Marine-Earth Science and Technology, Yokosuka, Japan, [4]MARUM, Center for Marine Environmental Sciences, University of Bremen, Bremen, Germany, [5]Department of Environment, Earth and Ecosystems, Open University, Walton Hall, Milton Keynes, UK

Abstract Fossil fish teeth from pelagic open ocean settings are considered a robust archive for preserving the neodymium (Nd) isotopic composition of ancient seawater. However, using fossil fish teeth as an archive to reconstruct seawater Nd isotopic compositions in different sedimentary redox environments and in terrigenous-dominated, shallow marine settings is less proven. To address these uncertainties, fish tooth and sediment samples from a middle Eocene section deposited proximal to the East Antarctic margin at Integrated Ocean Drilling Program Site U1356 were analyzed for major and trace element geochemistry, and Nd isotopes. Major and trace element analyses of the sediments reveal changing redox conditions throughout deposition in a shallow marine environment. However, variations in the Nd isotopic composition and rare earth element (REE) patterns of the associated fish teeth do not correspond to redox changes in the sediments. REE patterns in fish teeth at Site U1356 carry a typical mid-REE-enriched signature. However, a consistently positive Ce anomaly marks a deviation from a pure authigenic origin of REEs to the fish tooth. Neodymium isotopic compositions of cleaned and uncleaned fish teeth fall between modern seawater and local sediments and hence could be authigenic in nature, but could also be influenced by sedimentary fluxes. We conclude that the fossil fish tooth Nd isotope proxy is not sensitive to moderate changes in pore water oxygenation. However, combined studies on sediments, pore waters, fish teeth, and seawater are needed to fully understand processes driving the reconstructed signature from shallow marine sections in proximity to continental sources.

1. Introduction

The preserved neodymium (Nd) isotopic composition of marine archives such as fossil fish teeth is commonly used in paleoceanographic studies to trace water masses and reconstruct circulation patterns [e.g., *Frank*, 2002; *Goldstein and Hemming*, 2003]. Neodymium is transferred to the oceans in both particulate and dissolved form from the weathering of surrounding continents via rivers and wind [e.g., *Lacan et al.*, 2012], with a significant loss in estuaries [e.g., *Goldstein and Jacobsen*, 1987; *Rousseau et al.*, 2015]. There is increasing evidence that exchange of Nd between sediments and seawater along ocean margins plays an important role in modifying the Nd isotope composition of water masses [e.g., *Carter et al.*, 2012; *Garcia-Solsona et al.*, 2014; *Lacan and Jeandel*, 2005; *Stichel et al.*, 2012; *Wilson et al.*, 2013]. Geological heterogeneity in areas of deep-water formation imparts distinct Nd isotope signatures on the composition of water masses that are formed in different areas of the oceans [e.g., *Jeandel et al.*, 2007]. These signatures can then be traced spatially due to the short residence time of Nd in the seawater (~400—1000 years) [*Tachikawa et al.*, 2003], indicating that away from ocean margins Nd isotope values of seawater are a quasiconservative water mass tracer.

Past seawater Nd isotopic compositions are recorded in several geological archives, including ferromanganese crusts and coatings, foraminifera, deep-sea corals, and fish teeth and debris [see *van de Flierdt and Frank*, 2010 for a recent summary]. Among these archives, fossil fish teeth are considered one of the most

robust recorders of seawater Nd. Rare earth elements (REEs) including Nd are incorporated into fossil fish teeth and debris post mortem during fossilization from apatite to hydroxyfluorapatite and the early sediment burial process [*Martin and Haley*, 2000; *Shaw and Wasserburg*, 1985; *Staudigel et al*., 1985]. Exchange of REEs with Ca in the apatite matrix, (accompanied by charge balancing substitution of cations or anions) forms insoluble REE phosphates and fluorides [e.g., *Arrhenius et al*., 1957]. This process generally occurs during early diagenesis at the sediment-water interface and in the upper few centimeters of the sediment [*Bernat*, 1975; *Elderfield and Pagett*, 1986; *Martin and Haley*, 2000; *Reynard et al*., 1999; *Sholkovitz et al*., 1989; *Staudigel et al*., 1985]. It is worth noting however, that in settings with higher sedimentation rates, the fossilization process may continue at slightly increased depths. As the concentration of REEs in fossil fish teeth does not significantly change in the sediment column with burial depth, it has been suggested that Cenozoic to recent-aged fish teeth preserve a primary seawater REE signal and that the Nd isotopic composition of fish teeth reflects ambient bottom water [*Martin and Haley*, 2000; *Martin and Scher*, 2004, *Tütken and Vennemann*, 2011]. However, *Kocsis et al*. [2010] showed that gradual diagenetic overprinting of REEs in fossil bioapatite could occur in samples of Cretaceous to Triassic age, suggesting a more open-exchange system than previously assumed in this fossil archive.

The majority of recent studies utilizing Nd isotopes in fish teeth as an ancient seawater archive are based on samples from pelagic open ocean locations with well-oxygenated seafloor conditions. In such locations, bottom waters (and early diagenetic pore fluids) record a deep-water Nd isotope signal and therefore provide information on large-scale ocean circulation patterns [e.g., *Martin and Scher*, 2006; *Scher and Martin*, 2004, 2008; *Thomas et al*., 2008, 2014]. However, Nd isotopes in fish teeth have also been used as a water mass tracer across major climate events characterized by rapid changes in deep-water and sedimentary redox conditions, such as the Mesozoic Oceanic Anoxic Events (OAEs) [e.g., *MacLeod et al*., 2008, 2011; *Martin et al*., 2012; *Robinson and Vance*, 2012; *Robinson et al*., 2010] and to reconstruct seawater compositions at shallow marine sites [e.g., *Charbonnier et al*., 2012; *Moiroud et al*., 2013; *Pucéat et al*., 2005]. Shallow water sites are particularly important locations for reconstruction of past circulation states during the Mesozoic when epicontinental seas were more widespread then today. Shallow water sites are also important for reconstruction of the opening/closure of oceanic gateways [e.g., *Bijl et al*., 2013]. To our knowledge, no study has so far tested the robustness of the Nd isotope proxy as water mass tracer under (i) variable redox conditions, and (ii) in shallow marine environments.

Neodymium, along with the other REEs in seawater and pore waters, is derived from dissolved and particulate phases. Dissolved Nd may be delivered to a specific location via proximal sources such as rivers or via advection of water masses formed elsewhere. Particulate Nd may also contribute to the dissolved Nd budget through dissolution, as documented for areas dominated by volcanic particulates and in estuaries [e.g., *Pearce et al*., 2013; *Rousseau et al*., 2015]. Fish teeth, iron-manganese (FeMn) oxides/oxyhydroxides [*Bau et al*., 1996; *Haley et al*., 2004] and sedimentary organic matter coatings (SOM) [*Freslon et al*., 2014; *Haley et al*., 2004], incorporate dissolved REEs and are assumed to represent an in situ, bottom water composition [e.g., *Bayon et al*., 2002; *Gutjahr et al*., 2007; *Roberts et al*., 2010; *Rutberg et al*., 2000]. However, Fe and Mn are both redox sensitive elements, and formation and dissolution of FeMn coatings in pore waters may hence be affected by variable redox conditions during the depositional history of a sedimentary sequence. This means that coatings themselves may become a source of REEs to the pore water or incorporate dissolved REEs from multiple sources such as the host sediments and the ambient seawater during formation [*Abbott et al*., 2015]. Therefore, both the study location (e.g., shallow marine versus deep ocean) and sediment redox conditions may influence the elemental composition of pore waters.

In this study, we examine the robustness of fossil fish tooth Nd isotopes as a water mass proxy within an Eocene shallow marine section that underwent distinct changes in redox conditions. We use material from IODP Site U1356, from the Wilkes Land Margin of the Antarctic continent. Physical property (a*; red/green color reflectance data), grain size, fish tooth abundance, and X-ray Fluorescence (XRF) scan data of the sediments at Site U1356 are utilized to establish the depositional environment during our study interval. To further characterize sedimentary and geochemical processes within the section, we analyzed the Nd isotopic composition, REE patterns, and major and trace element geochemistry of fish teeth and the bulk sediment hosting the fish teeth. We find that Nd isotope values of fossil fish teeth and sediments remain distinct downcore, and that fish tooth REE patterns indicate a pore water origin. This suggests that at Site U1356, fish teeth are not overprinted by sedimentary fluxes and record an authigenic signal; however, a consistently positive cerium (Ce) anomaly throughout changing redox layers may indicate an additional control

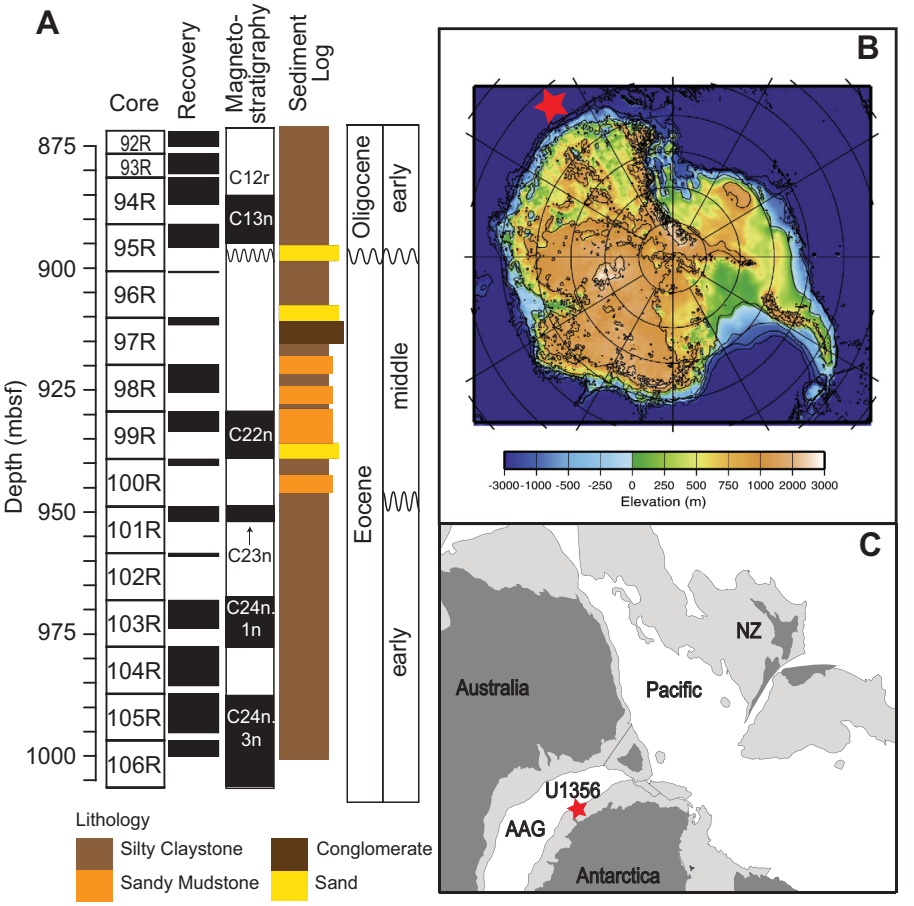

Figure 1. (a) Lithostratigraphic column of the late Oligocene to early Eocene interval of Wilkes Land IODP Site U1356 (adapted from *Escutia et al.* [2011]), including core recovery and ages (magnetostratigraphic data taken from *Tauxe et al.* [2012]). (b) Site location (red star) plotted on the Eocene topographical reconstruction of *Wilson et al.* [2012]. (c) Paleolocation of study Site U1356 on the Wilkes Land margin (adapted from *Bijl et al.* [2013]). AAG = Australo-Antarctic Gulf, NZ = New Zealand. White areas of deeper seawater in the Pacific and the Australo-Antarctic Gulf are separated by the Tasmanian Gateway, connecting the landmasses of Australia and Antarctica in the early Eocene.

on fish tooth chemistry in shelf settings. Finally, downcore changes in Nd isotopes of the sediment and fish teeth do not correlate with changing redox conditions within the sediments at Site U1356.

2. Setting and Samples

Integrated Ocean Drilling Program (IODP) Site U1356 was drilled during Expedition 318 off the Adélie/Wilkes Land coast of Antarctica (63°18′S, 135°59′E) and is currently located at a water depth of 4003 m [*Escutia et al.*, 2011] (Figure 1). The hole was drilled to a depth of 1006 m below seafloor (mbsf), and the lowermost 110 m consist of a well-dated lower-to-middle Eocene section [*Tauxe et al.*, 2012] (Figure 1). The lower Eocene sediments (949–1000 mbsf; ~51–54 Ma) consist mainly of heavily bioturbated silty claystones and claystones. A hiatus separates the lower and middle Eocene sections. Middle Eocene (890–945 mbsf; ~46–49 Ma) sediments consist of interbedded sandstones, conglomerates, silty claystones, and siltstones. For our study, we focused on the middle Eocene interval of Hole U1356A between 920 and 926 mbsf (Core 318-U1356A-98R; ~48–49 Ma). Core U1356A-98R is distinguished from underlying and overlying strata by the occurrence of reddish-brown silty claystones interbedded with greenish-gray and brown sandy mudstones at the centimeter to decimeter scale (Figure 2). These layers with alternating colors (referred to as "red" and "green" for the remainder of the text) are distinct and clearly depicted in shipboard measurements of a* (Figure 2) [*Escutia et al.*, 2011].

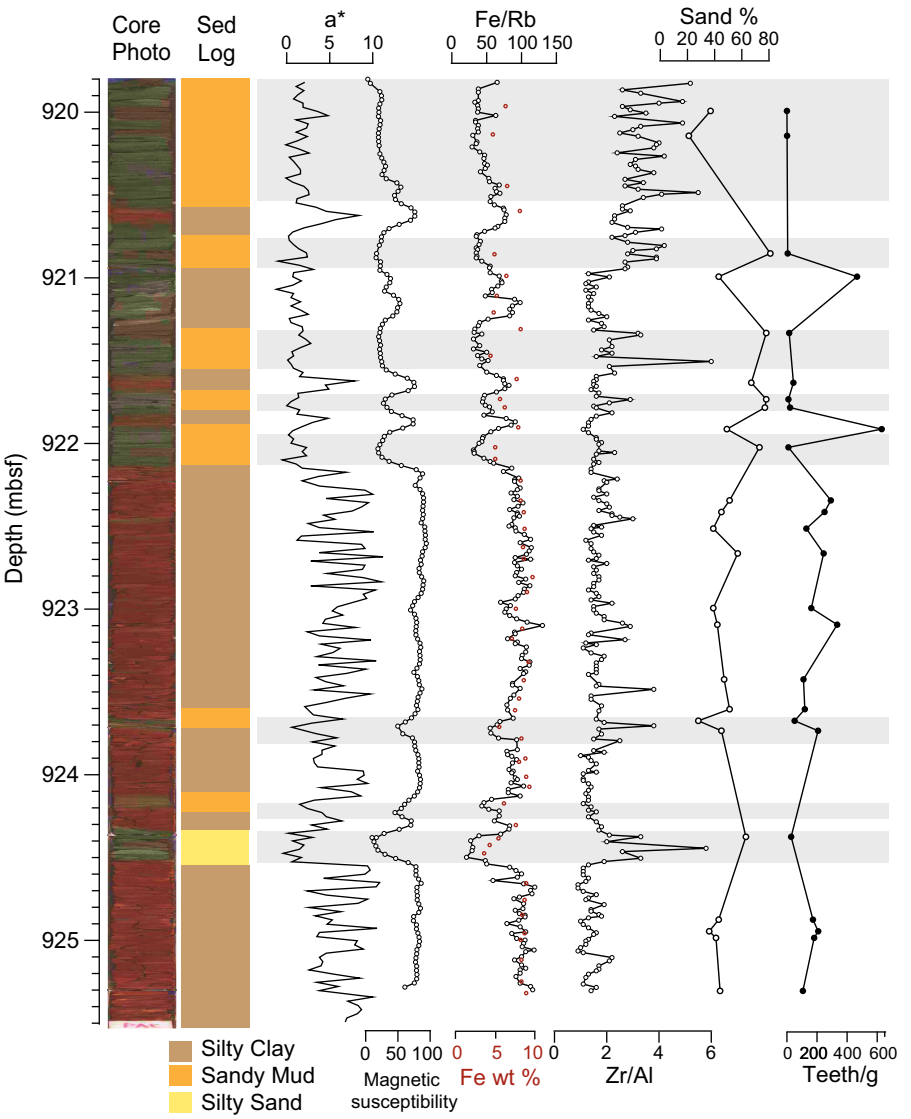

Figure 2. Core photo, color reflectance data (a*– red/green ratio), sedimentary log and magnetic susceptibility data (modified after *Escutia et al.* [2011]). Fe/Rb and Zr/Al XRF ratios, Fe wt. % data from discrete sample measurement, and sand % and fish tooth/g data from the >63 μm fraction of samples washed for Nd isotopic analysis. Gray horizontal shading represents green layers as identified by their low magnetic susceptibility and a* reflectance values.

3. Methods

3.1. Bulk Sediment Analyses

3.1.1. Major and Trace Element Concentrations of Bulk Sediments

Major and trace element analyses of 50 sediment samples from Core U1356A-98R (36 from red layers and 14 from green layers) were performed at the University of Granada. Samples for trace element analyses (~100 mg) were digested in sealed teflon vials overnight in concentrated HNO_3 and HF at 120°C on a hot-plate. Major elements were measured by Wavelength Dispersive XRF Spectrometry (Bruker AXS S4 Pioneer with an Rh anode X-ray tube) on pressed pellets, with an analytical detection limit of 0.1% and an instrumental error <1%. Trace element analyses were performed on splits of the same samples by Inductively Coupled Plasma-Mass Spectrometry (ICP-MS) using a Perkin Elmer Sciex Elan 5000, with an instrumental uncertainty of ± 2% for elemental concentrations above 50 ppm and ±5% for concentrations between 50 and 5 ppm, respectively [*Bea et al.*, 1996] (Table 1). For quality control, reference geostandards UBN, PMS, WSE, BEN, BR, AGV, DRN, GSN GA, and GH were analyzed alongside the samples, and Re and Rh (25 ppb) were used as internal standards [*Govindaraju*, 1994].

Table 1. Rare Earth Element Concentration Data for Fossil Fish Tooth and Bulk Sediment Samples (ppm)[a]

Fish Tooth Sample	Depth (mbsf)	La	Ce	Pr	Nd	Sm	Eu	Gd	Tb	Dy	Y	Ho	Er	Tm	Yb	Lu	Sediment Color	ΣREE
318-U1356A-98R-1, 0811[b]	919.90	1057.1	3697.4	352.7	1515.9	372.5	93.0	428.8	64.9	405.0	2269.9	79.3	223.1	28.4	166.5	24.8	G	10779.3
318-U1356A-98R-1, 0811[c]	919.90	334.1	1009.3	107.7	460.9	114.5	26.7	128.4	20.1	124.8	688.8	25.1	69.8	9.4	53.6	7.9	G	3181.1
318-U1356A-98R-1, 4144	920.24	432.2	1475.6	159.1	683.7	175.5	41.6	194.8	30.8	192.3	1003.4	38.3	106.8	13.9	84.8	12.5	G	4645.3
318-U1356A-98R-1, 8084	920.64	509.9	1724.1	185.8	785.4	200.4	48.5	224.3	35.0	222.3	1171.9	43.9	125.7	16.2	95.7	14.3	R	5403.4
318-U1356A-98R-2, 0003	920.96	953.8	2650.6	291.1	1206.7	278.8	66.4	311.5	48.0	310.3	1793.5	62.8	182.4	24.3	143.8	21.4	G	8345.4
318-U1356A-98R-2, 5861[b]	921.55	737.1	2749.8	274.6	1166.9	294.5	66.5	310.6	47.9	296.0	1627.0	58.5	161.5	20.8	119.5	17.5	G	7948.7
318-U1356A-98R-2, 5861[c]	921.55	438.8	1502.9	154.5	656.4	162.7	38.5	179.9	27.8	173.8	984.2	35.3	98.7	12.9	76.7	11.2	G	4554.4
318-U1356A-98R-2, 120123	922.17	583.1	1858.9	181.0	740.1	174.5	40.8	195.2	29.6	192.2	1127.2	39.2	116.3	15.5	93.2	13.8	R	5400.7
318-U1356A-98R-3, 4043	922.66	713.4	2553.2	237.5	960.9	226.3	53.4	242.5	37.4	241.0	1323.8	48.0	137.6	18.7	111.0	16.3	R	6921.1
318-U1356A-98R-3, 100103[b]	923.24	638.8	2096.4	191.1	768.2	171.8	39.7	184.2	27.8	179.7	1065.4	36.2	106.5	14.4	85.9	12.4	R	5618.4
318-U1356A-98R-3, 100103[c]	923.24	550.1	1840.6	172.1	696.3	163.4	37.6	173.8	27.2	175.5	1034.8	35.6	106.6	14.1	86.5	13.1	R	5127.2
318-U1356A-98R-3, 120123	923.44	836.5	2615.0	247.6	1007.9	226.2	52.4	243.6	36.8	231.3	1325.4	46.6	133.9	17.6	103.0	14.9	R	7138.6
318-U1356A-98R-4, 2529	923.98	579.3	1776.8	169.0	684.0	152.3	36.2	167.0	25.1	162.9	925.0	32.7	96.5	13.5	79.5	11.9	R	4911.6
318-U1356A-98R-4, 4246	924.18	553.8	1821.9	177.8	709.1	161.6	37.4	171.6	25.8	162.3	877.7	32.1	94.3	12.6	74.1	10.8	G	4922.8
318-U1356A-98R-4, 6063	924.38	410.8	1517.2	138.6	566.8	127.0	29.9	135.3	20.2	126.7	651.6	24.7	70.2	9.3	53.0	8.1	G	3889.3
318-U1356A-98R-5, 0003	924.40	380.4	1516.6	138.8	553.3	130.2	28.6	139.1	20.7	127.2	637.8	24.3	72.2	9.3	57.3	8.3	G	3844.2
318-U1356A-98R-5, 6063	925.00	698.7	2379.9	214.0	863.9	196.6	44.9	213.3	31.9	204.5	1202.6	41.4	119.6	16.7	101.7	14.8	R	6344.4
318-U1356A-98R-5, 8083[b]	925.20	305.4	795.0	84.9	339.8	75.8	17.0	80.4	12.0	75.2	451.0	15.2	46.4	6.4	40.1	6.1	R	2350.6
318-U1356A-98R-5, 8083[c]	925.20	75.4	183.9	19.7	79.8	17.6	3.9	18.6	2.8	17.5	113.7	3.7	11.3	1.5	9.9	1.5	R	561.0
Bulk Sediment Sample																		
Average "Red"		36.2	78.6	8.3	30.7	6.1	1.3	5.4	0.9	4.7	27.4	1.0	2.6	0.4	2.7	0.4	R	
Average "Green"		33.7	73.5	7.9	29.7	5.9	1.2	5.0	0.8	4.3	23.5	0.9	2.3	0.4	2.4	0.4	G	

[a]Full bulk sediment REE data can be found in supporting information. Precision of ±5% for sediment samples, and ±2% for fish tooth samples. Sediment color R=Red; G=Green.
[b]Denotes uncleaned sample subject to cleaning with only MQ water and methanol.
[c]Denotes cleaned sample subject to full oxidative-reductive cleaning protocol.

For the acquisition of high-resolution elemental intensity data (Al through Ba), we used the XRF Core Scanner III (AVAATECH Serial No. 12) at the MARUM, University of Bremen. XRF Core Scanner data were collected every 2 cm downcore over a 1 cm^2 area in three separate runs using generator settings of 10, 30, and 50 kV, currents of 0.2, 1.5, and 1.5 mA, respectively, and a down-core slit size of 10 mm. These data are included in supporting information.

3.1.2. Neodymium Isotopic Composition of Bulk Sediments

The Nd isotopic composition of six bulk sediment samples from Core U1356A-98R (four from red layers and two from green layers) was determined at Imperial College London (Table 2). Approximately 1.0 g of bulk sediment was homogenized using a pestle and mortar before removing a ~100 mg aliquot for analysis. Authigenic FeMn oxyhydroxide and biogenic phases were not removed prior to digestion because the study section is predominantly terrigenous in composition [>97%; *Escutia et al.*, 2011]. Samples were digested on a hotplate using a mixture of 0.5 mL 20*M* $HClO_4$, 1 mL 15*M* HNO_3 and 3 mL 27*M* HF, and subjected to a standard two-stage ion chromatography procedure. A first column using Eichrom TRU Spec resin (100–120 μm bead size) was utilized to isolate the REEs from the sample matrix, and a second column with Eichrom Ln-Spec resin (50–100 μm bead size) was utilized to separate Nd from the other REEs (slightly modified after *Pin and Zalduegui* [1997]). Procedural blanks were included in all sample preparation batches and were consistently below 10 pg Nd.

Neodymium isotope ratios were measured on a Nu Plasma MC-ICP-MS at Imperial College London in static mode. Instrumental mass bias was corrected for using a $^{146}Nd/^{144}Nd$ ratio of 0.7219. Samarium (Sm) interference can be adequately corrected if the ^{144}Sm signal contributes less than 0.1% of the ^{144}Nd signal. The Sm contribution in all our samples (fish teeth and sediments) was well below this level. Replicate analyses of the Nd standard JNdi yielded $^{143}Nd/^{144}Nd$ ratios of 0.511937 (±0.000015, n = 16) and 0.512147 (±0.000010, n = 16) over two measurement sessions. All samples within each measurement session were corrected for the offset between the recorded and documented value for JNdi (0.512115) [*Tanaka et al.*, 2000]. External reproducibility of the method was monitored using USGS rock standard BCR-1, which yielded 0.512651 ± 0.000014. This value is identical within error to the TIMS value of 0.512638 ± 0.000006 published by *Weis et al.* [2006]. All Nd isotope data are expressed in the $\varepsilon_{Nd(t)}$ notation (ε_{Nd} is the deviation of the sample $^{143}Nd/^{144}Nd$ ratio from the chondritic uniform reservoir (CHUR) at the time of deposition in parts per 10,000; $_{(t)}$ denotes samples have been corrected for in situ decay of ^{147}Sm (section 3.3)).

Table 2. Neodymium Isotope Data for Fish Tooth and Sediment Samples[a]

Sample Name	Depth (mbsf)	$^{143}Nd/^{144}Nd$[b]	± 2σ S.E[c]	ε_{Nd}[d]	± 2σ S.D[e]	$^{147}Sm/^{144}Nd$[f]	$\varepsilon_{Nd(t)}$[g]	Sediment Color
Fish Teeth								
318-U1356A-98R-1, 0811[h]	919.90	0.512049	0.000010	−11.5	0.2	0.155	−11.2	G
318-U1356A-98R-1, 0811[i]	919.90	0.512035	0.000012	−11.8	0.3	0.155	−11.5	G
318-U1356A-98R-1, 4144	920.24	0.512049	0.000010	−11.5	0.2	0.162	−11.3	G
318-U1356A-98R-1 6468	920.44	0.512083	0.000029	−10.8	0.3	*0.153*	−10.5	G
318-U1356A-98R-1, 8084	920.64	0.512067	0.000010	−11.1	0.2	0.161	−10.9	R
318-U1356A-98R-2, 0003	920.96	0.512047	0.000008	−11.5	0.2	0.146	−11.2	G
318-U1356A-98R-2, 5861[h]	921.55	0.512071	0.000014	−11.1	0.2	0.159	−10.8	G
318-U1356A-98R-2, 5861[i]	921.55	0.512072	0.000016	−11.0	0.2	0.159	−10.8	G
318-U1356A-98R-2, 120123	922.17	0.512060	0.000012	−11.3	0.3	0.148	−11.0	R
318-U1356A-98R-3, 4043	922.66	0.512041	0.000010	−11.7	0.2	0.148	−11.4	R
318-U1356A-98R-3, 5559	922.81	0.512038	0.000027	−11.7	0.3	*0.153*	−11.4	R
318-U1356A-98R-3, 100103[h]	923.24	0.512032	0.000014	−11.8	0.2	0.141	−11.5	R
318-U1356A-98R-3, 100103[i]	923.24	0.512026	0.000018	−11.9	0.2	0.141	−11.6	R
318-U1356A-98R-3, 120123	923.44	0.512008	0.000006	−12.3	0.2	0.141	−11.9	R
318-U1356A-98R-4, 2529	923.98	0.512006	0.000008	−12.3	0.2	0.140	−12.0	R
[j]318-U1356A-98R-4, 2529	923.98	0.512009	0.000023	−12.3	0.2	0.140	−11.9	R
318-U1356A-98R-4, 4246	924.18	0.512019	0.000010	−12.1	0.3	0.144	−11.7	G
318-U1356A-98R-4, 6063	924.38	0.512020	0.000012	−12.1	0.3	0.141	−11.7	G
318-U1356A-98R-5, 0003	924.40	0.512035	0.000012	−11.8	0.3	0.148	−11.5	G
318-U1356A-98R-5, 2529	924.63	0.512020	0.000023	−12.1	0.3	*0.153*	−11.8	R
[k]318-U1356A-98R-5, 2529	924.63	0.512011	0.000014	−12.2	0.3	*0.153*	−12.0	R
318-U1356A-98R-5, 6063	925.00	0.512006	0.000008	−12.3	0.2	0.143	−12.0	R
318-U1356A-98R-5, 7074	925.10	0.512022	0.000023	−12.0	0.3	*0.153*	−11.7	R
318-U1356A-98R-5, 8083[h]	925.20	0.511984	0.000014	−12.8	0.3	0.141	−12.4	R
318-U1356A-98R-5, 8083[i]	925.20	0.511980	0.000016	−12.8	0.3	0.141	−12.5	R
Sediments								
318-U1356A-98R-1, 6468	920.44	0.511865	0.000014	−15.1	0.3	*0.126*	−14.6	G
318-U1356A-98R-2, 0003	920.96	0.511921	0.000014	−14.0	0.3	*0.126*	−13.6	G
318-U1356A-98R-3, 0003	922.26	0.511908	0.000012	−14.2	0.3	*0.126*	−13.9	R
318-U1356A-98R-4, 2024	923.93	0.511872	0.000013	−14.9	0.3	*0.126*	−14.5	R
318-U1356A-98R-5, 2024	924.58	0.511871	0.000016	−15.0	0.3	*0.126*	−14.5	R
318-U1356A-98R-5, 79.5	925.18	0.511875	0.000014	−14.9	0.3	*0.126*	−14.5	R

[a]Repeat analyses of JNdi standard range from 0.512005 (±0.000012) to 0.512147 (±0.000010) for fish teeth and 0.511937 (±0.000015) to 0.512147 (±0.000010) for sediments. Sediment color R = Red; G = Green.
[b]Measured Nd isotopic composition normalized to JNdi $^{143}Nd/^{144}Nd$ value of 0.512115 [*Tanaka et al.*, 2000].
[c]Internal 2σ standard error of the measurements.
[d]ε_{Nd} values are calculated relative to CHUR value of 0.512638 [*Jacobsen and Wasserburg*, 1980].
[e]External errors are the 2σ standard deviations derived from repeat analyses of the JNdi standard. Uncertainties plotted in Figure 5 are 2σ S.E. or 2σ S.D, dependant on which one is larger.
[f]$^{147}Sm/^{144}Nd$ ratio calculated from REE concentration measurement (Table 1). Where no value was available, an average value of 0.153 (fish teeth) or 0.126 (sediments) was used and is reported in italic font.
[g]$\varepsilon_{Nd(t)}$ values calculated using $^{147}Sm/^{144}Nd$ values from column f, and CHUR values of $^{143}Nd/^{144}Nd$=0.512638; $^{147}Sm/^{144}Nd$=0.1966 [*Jacobsen and Wasserburg*, 1980].
[h]Denotes uncleaned sample subject to cleaning with only MQ water and methanol.
[i]Denotes cleaned sample subject to full oxidative-reductive cleaning protocol.
[j]Denotes full chemical replicate.
[k]Denotes chemical duplicate.

3.2. Fossil Fish Teeth and Debris Analyses

3.2.1. Sample Preparation

The Nd isotopic composition of 19 fish tooth samples from Core U1356A-98R (12 from red layers and seven from green layers) was determined at Imperial College London (Table 2). Between 10 and 30 cm^3 of sediment was oven dried at 60°C, soaked in deionized water to disaggregate, and sieved through a 63 μm mesh. Fish tooth and bone debris were handpicked from the >63 μm fraction with a minimum target weight of 150 μg in order to obtain enough Nd (>10 ng) for analysis. The teeth and debris were then cleaned with ultrapure Milli-Q water (18.2 MΩ water) and methanol following the simple cleaning method in *Martin and Haley* [2000]. In addition, four samples were split before cleaning, with one aliquot cleaned as described above, and the other aliquot subjected to a full oxidative-reductive cleaning protocol to remove FeMn oxyhydroxide coatings (method adapted from *Boyle and Keigwin* [1987]). The oxidative reagents consisted of a 0.1% solution of sodium hydroxide and hydrogen peroxide. The reductive solution consisted of

citric acid, ammonium hydroxide, and hydrazine for a target concentration of 4%. These sample splits are referred to hereafter as "uncleaned" and "cleaned," respectively (see Table 2). All samples were dissolved in 2*M* HCl.

3.2.2. Major and Trace Element Concentrations of Fossil Fish Teeth

A 10% aliquot of the digested fossil fish tooth sample solution was taken for major and trace element analyses using an Agilent 7500s ICP-MS at the Open University (Table 1). Oxide interferences were kept below 0.3% for CeO^+/Ce^+ and at 0.8% for (Ce^{++}/Ce^+). Analyses were standardized against seven synthetic reference materials selected for their similarity to the samples that were measured at the beginning and end of each analytical run. Detection limits for elements with atomic masses greater than 85 were typically $<$10 ppt in solution but somewhat higher for lighter elements (10–100 ppt in solution). Precision was routinely better than $\pm$2% for elements heavier than rubidium (Rb) (where concentrations exceed 0.5 ppm) and 2–4% for elements lighter. Full major and trace element data are supplied in the supporting information.

3.2.3. Neodymium Isotopic Composition of Fossil Fish Teeth

Digested fish tooth samples were processed and analyzed using the same column chemistry and mass spectrometry as outlined above for bulk sediments. Replicate analyses of the Nd standard JNdi yielded $^{143}Nd/^{144}Nd$ ratios from 0.512005 ($\pm$0.000012) to 0.512147 ($\pm$0.000010) (n = 102), dependent on daily running conditions from seven measurement sessions over 21 months.

The external reproducibility of Nd isotope measurements was monitored using a fossil bone composite standard, yielding 0.512377 $\pm$ 0.000028 (n = 8; over 18 months), which is the same within error as results published by *Chavagnac et al*. [2007] and *Scher and Delaney* [2010]. For consistency with previous studies, the fossil bone standard was digested differently to our fossil fish tooth samples, following the method described in *Chavagnac et al*. [2007]. 50 mg of material was digested in 3*M* HNO_3 at 130°C for 24 h, and all supernatant removed, dried down, and converted to chloride form. Any residue was then treated using a 3:1 mixture of concentrated HF and HNO_3 on a hotplate at 130°C for up to a further 48 h. The residue was then recombined with the supernatant cut before the same chemistry procedure described above was followed. Full chemical replicates and duplicate analyses of samples yielded results within error (Table 2).

3.3. Age Correction for ε_{Nd} Values

To correct for the decay of ^{147}Sm to ^{144}Nd within the fish teeth and sediments since deposition, we used the REE concentrations obtained for the 19 individual fish teeth samples and 50 bulk sediment samples to calculate $^{147}Sm/^{144}Nd$ ratios. CHUR values for the present day were taken from *Jacobsen and Wasserburg* [1980] ($^{143}Nd/^{144}Nd = 0.512638$; $^{147}Sm/^{144}Nd = 0.1966$). Fish tooth $^{147}Sm/^{144}Nd$ ratios ranged from 0.141 to 0.162 (Table 1), which resulted in a Nd isotope correction of $\sim$0.3 ε_{Nd} units, similar to that reported in other studies [*Martin and Scher*, 2006; *Moiroud et al*., 2013; *Thomas et al*., 2003]. For fish tooth samples that did not have REE concentrations measured, an average value of the measured samples (0.153) was taken and applied. Sediment $^{147}Sm/^{144}Nd$ ratios of between 0.119 and 0.133 fall within the range recorded by other studies from the Wilkes Land area [e.g., *Borg and DePaolo*, 1991; *Turner et al*., 1993]. An average value of our samples was taken (0.126) and applied to additional samples not analyzed for major and trace elements, but analyzed for their Nd isotopic composition.

4. Results

4.1. Major and Trace Element Concentrations and XRF Ratios of Bulk Sediments

Iron (Fe) concentrations within the U1356A study section vary between 3.6 and 9.7 wt. % and covary with Fe/Rb XRF ratios, sediment color, and magnetic susceptibility data downcore (Figure 2). Higher percentages of sand and higher zirconium/aluminium (Zr/Al) ratios are associated with green layers, which contain lower Fe concentrations. Lower percentages of sand in the sediments and lower Zr/Al ratios in turn correspond to Fe-rich red layers and high abundances of fossil fish teeth (Figure 2). Variations in the concentration of redox sensitive elements including uranium (U), copper (Cu), zinc (Zn), and cobalt (Co) are anticorrelated with Fe concentrations (Figure 3). Iron-poor layers are furthermore characterized by concentrations of U, Cu, Zn and Co that exceed their average crustal content (Figure 3) [*Taylor and McLennan*, 1985]. The sulphur (S) content, assessed by the XRF ratio S/Ti (Figure 3), also shows higher values within the Fe-poor green layers.

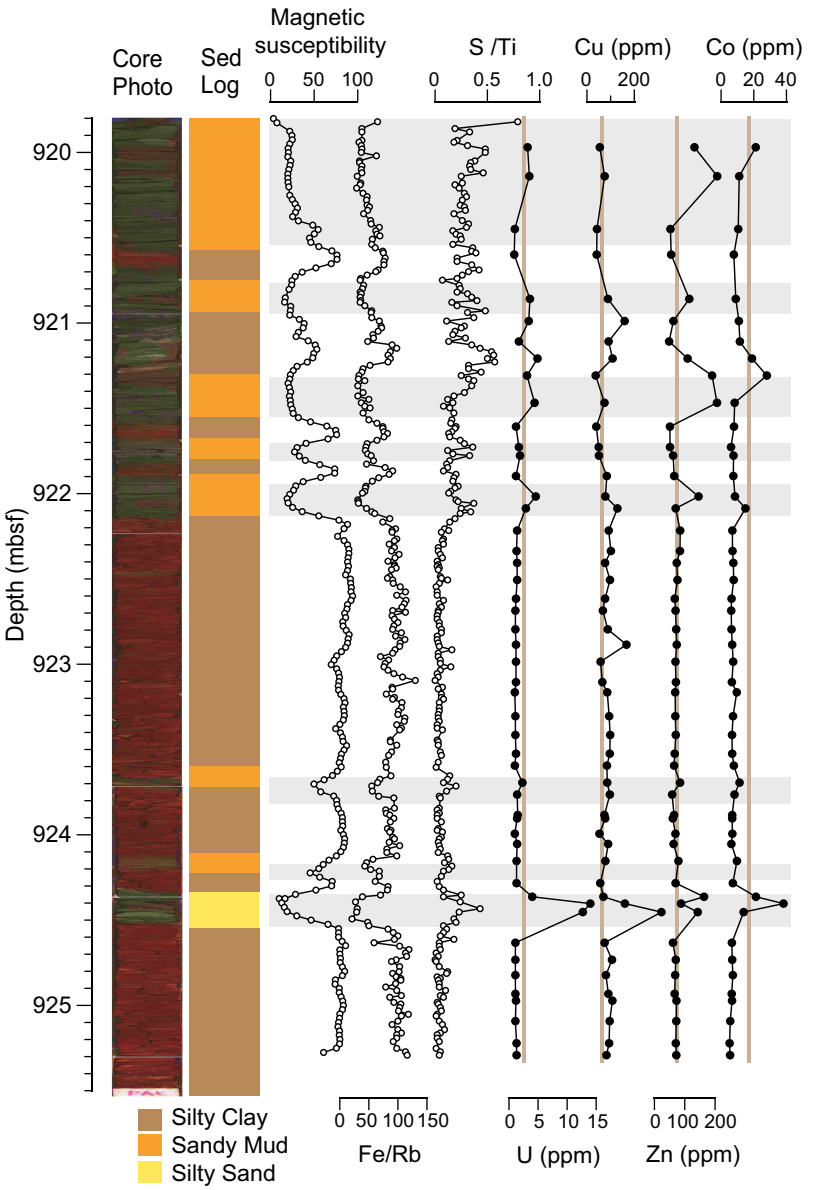

Figure 3. Core photo, sedimentary log, and magnetic susceptibility data (modified after *Escutia et al.* [2011]). Fe/Rb and S/Ti XRF ratios and trace metal concentrations from discrete ICP-MS analysis. Average crustal concentration of trace elements indicated with horizontal brown lines [*Taylor and McLennan*, 1985].

4.2. Major and Trace Element Concentrations of Fossil Fish Teeth

Average concentrations of most major and trace elements in fish tooth samples from Site U1356 are significantly lower than those in their host sediments (e.g., $[Fe]_{sediment} = 7\%$ versus $[Fe]_{fish\ teeth} = 0.8\%$). However, elements such as strontium (Sr), barium (Ba), Zn, and U are significantly enriched in fish teeth relative to sediments, and typically occur in their highest abundances within the green sediment layers (Figure 4). Aluminium levels are consistently below 0.4%, with the exception of Sample U1356A-98R-5, 0003 (924.40 mbsf), where Al concentrations reach almost 9%. High concentrations of Al in a seawater archive such as a fossil fish tooth are indicative of contamination, as natural dissolved levels of Al in seawater are extremely low. This sample is therefore excluded from further discussion.

4.3. Neodymium Isotopic Composition of Bulk Sediments and Fossil Fish Teeth

Core U1356A-98R bulk sediment Nd isotope values vary by just over 1 epsilon unit from −13.6 to −14.6 and subtle variations in $\varepsilon_{Nd(t)}$ do not correlate with sediment lithology, color, and/or elemental

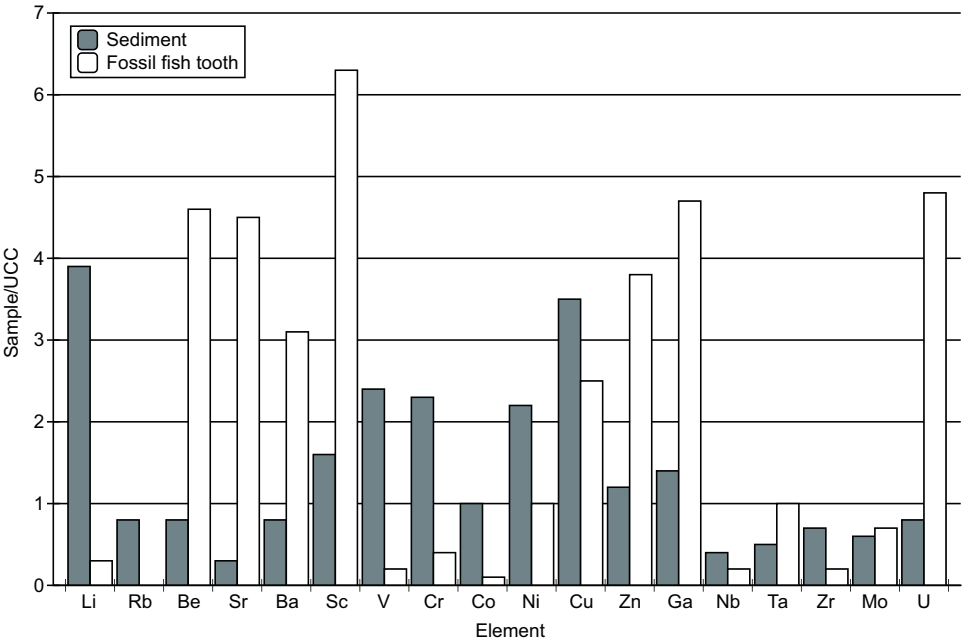

Figure 4. Average trace element data from fossil fish tooth (white bars) and sediment samples (gray bars) normalized to Upper Continental Crust (UCC) [*Taylor and McLennan*, 1985].

concentration, although the sampling resolution is low (n = 6) (Figure 5). Neodymium isotopic compositions in fossil fish teeth from the U1356 study section span a range of 2 epsilon units from −10.5 to −12.5 (Table 2, Figure 5). No systematic relationship is observed between lithology, sediment color, and/or elemental concentrations and fish tooth $\varepsilon_{Nd(t)}$ values. Importantly, the $\varepsilon_{Nd(t)}$ values of bulk sediments and fish teeth are distinct throughout the core, with bulk sediments yielding Nd isotopic compositions 2.0–2.4 epsilon units lower than fish teeth and debris. However, both records also display a downcore trend to more unradiogenic values (Figure 5). As sediment samples were not leached before digestion, there is the possibility of a minor contribution of Nd from FeMn coatings (a maximum of 20%) [*Gutjahr et al*., 2007], however we consider this unlikely when combined with REE pattern data below (section 4.4). The four samples consisting of splits of fully cleaned and uncleaned (water and methanol only) fossil teeth and debris produced the same Nd isotopic composition within error (Table 2).

4.4. REE Patterns of Bulk Sediments and Fossil Fish Teeth

Fossil fish tooth (n = 19) and sediment sample (n = 50) REE results from Core U1356A-98R samples were normalized to PAAS (Post Archean Average Shale) [*Taylor and McLennan*, 1985] (Table 1 and Figure 6). The sediment samples show a relatively flat REE profile (La/Yb = 1.01), which is characteristic of shale, in both the red and green sediment layers of Core U1356A-98R (Figure 6). In contrast, the REE patterns of fish teeth extracted from both the red and green lithologies are characterized by a middle REE (MREE; Gd, Tb, and Dy) enrichment and a positive Ce anomaly (where $Ce/Ce^* = 2Ce_n/(La_n+Pr_n)$; after *De Baar et al*. [1985]) (Figure 6). Fish tooth samples associated with green layers yielded higher REE concentrations than samples from the red layers (average $REE_{green} = 6339$ ppm, average $\Sigma REE_{red} = 5962$ ppm; Table 1; Figure 6). This enrichment occurs predominantly within the MREEs, with an average concentration of 510 ppm for fish teeth from green layers, compared with 446 ppm for fish teeth from red layers (Table 1). The REE profiles for the sample sets of cleaned and uncleaned fossil fish teeth (Figure 7) reveal that the REE pattern remains unchanged by the cleaning process, but that REE concentrations are consistently lower in cleaned samples relative to uncleaned ones. One set of sample pairs subjected to these different preparation methods (Sample U1356A-98R-5, 80-83 cm; Table 1), yielded unusually low REE concentrations for unknown reasons and is omitted in the following interpretation and discussion.

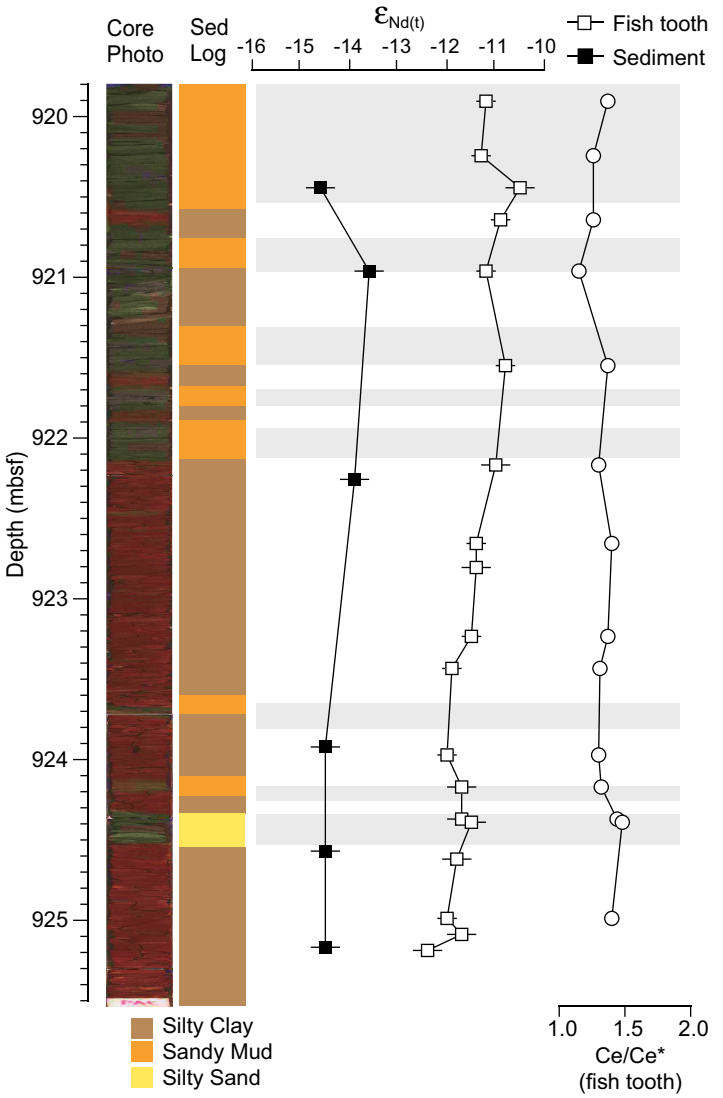

Figure 5. Reconstructed authigenic (white squares) and detrital (black squares) neodymium isotope composition from fossil fish tooth and sediment samples at IODP Site U1356, Core U1356A-98R. Ce/Ce* data for fish tooth samples calculated from REE data (Table 1).

5. Depositional Environment

5.1. Middle Eocene Depositional Setting of IODP Site U1356

The lower 110 m of the sedimentary section recovered at Site U1356 consists of lower and middle Eocene strata [*Escutia et al.*, 2011]. The sediments of early Eocene age (949–1006 mbsf; ~51–54 Ma) are dominated by bioturbated claystones with occasional muddy sandstone layers. Middle Eocene sediments (890–949 mbsf; ~46–Ma) are characterized by thick (up to ~1 m) sandstone and conglomerate beds containing pyrite and abundant intraclasts. Interspersed between these coarser beds are finer lithologies of sandy mudstones to silty claystones [*Escutia et al.*, 2011]. Soft sediment deformational features are found in the coarser sandstones and occasionally in the sandy mudstones, suggesting possible emplacement of these units via sediment gravity flows [*Bijl et al.*, 2013]. These coarser sandstone beds are almost entirely absent from both underlying (lower Eocene) and overlying (Oligocene) strata within Hole U1356A. The deposition of coarser sediments at Site U1356 during the middle Eocene is associated with a period of tectonic rifting and basin deepening in the Tasman Gateway region [*Close et al.*, 2009; *Escutia et al.*, 2011]. This led to changing depositional conditions at Site U1356 from a shallow marine setting during the Early Eocene (<500 m paleodepth) to a hemipelagic marine environment during the Oligocene (>1000 m paleo-depth) [*Bijl et al.*, 2013; *Escutia et al.*, 2011].

Core U1356A-98R (919.80–925.55 mbsf; ~48 to 49 Ma) is positioned stratigraphically within the middle Eocene section of Hole U1356A [*Escutia et al.*, 2011]. The sediments of Core U1356A-98R are characterized by interbedded sandy mudstones and silty claystones at a centimeter to decimeter scale. These different lithologies are also associated with alternation in sediment color, where coarser sediments are green and finer sediments are a distinctive red color (Figure 2). Sand content (>63 μm) is consistently lower in the silty claystones (red layers), which are associated with higher Fe/Rb XRF ratios (indicating Fe enrichment over the background sediment value) and high abundances of fossil fish teeth (up to 630 teeth/g) in comparison to the sandy mudstones (0–230 teeth/g; Figure 2). The coarser green intervals are also distinguished by increases in sand content, higher XRF ratios of Zr/Al, (Zr increases in concentration in silt/sand sized fractions of sediments), and lower ratios of Fe/Rb (Figure 2). Soft sediment deformation features can be

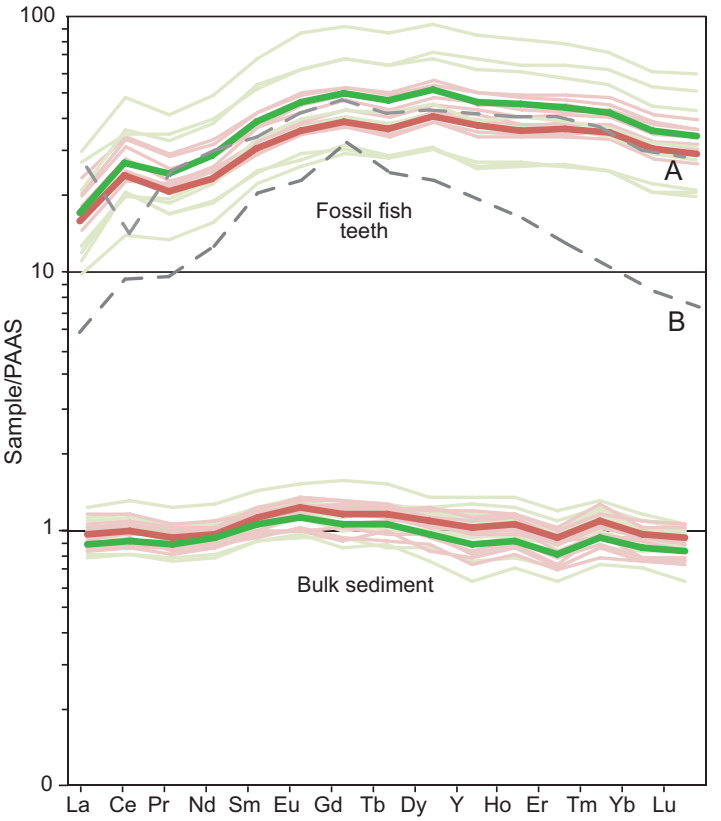

Figure 6. REE profiles of bulk sediment (bottom) and (top) fossil fish teeth, normalized to PAAS [*Taylor and McLennan*, 1985]. (a) Average open ocean fish tooth REE profile [*Martin et al*., 2010], (b) Average Cretaceous shelf site fish tooth REE profile [*Moiroud et al*., 2013].

observed within the sandy mudstones as well as a combination of sharp and gradational contacts between coarser and finer lithological units, again suggesting the influence of small-scale gravity flows.

In comparison to the other cores within the middle Eocene section of Hole U1356A, Core U1356A-98R contains only one thin interval of coarse sandstone (924.30–924.50 mbsf; Figure 2) and intervals of uninterrupted fine claystones up to ~1.5 m in thickness, which may represent quiescent periods between sediment gravity flow events. A consistent bulk sediment Nd isotopic composition across both main lithologies of Core U1356A-98R suggests that the sediments throughout this interval of Hole U1356A were supplied from the same source region (Figure 5). The coarser mudstone layers are the likely product of small sediment gravity flows, while the claystones may represent in situ deposition of fine-grained terrigenous material, all sourced from the adjacent coastline as indicated by their unradiogenic Nd isotopic composition.

5.2. Redox History of Core U1356A-98R

Distinct changes in sediment color banding, such as those observed in Core U1356A-98R (a* data; Figure 2), have been linked with the oxygenation state of the sediment pore waters in a range of marine environments [e.g., *Giosan et al*., 2002; *Potter et al*., 2005]. The chemistry of pore waters can be altered by changes in redox conditions with reducing sediment pore waters containing higher levels of remobilized REEs than oxic pore waters [e.g., *Bau et al*., 1997; *Elderfield and Sholkovitz*, 1987; *Haley et al*., 2004]. As the major control on REE incorporation into fish teeth during early diagenesis is the availability of REEs within the sediment pore waters [*Staudigel et al*., 1985], an interpretation of the sediment redox history is crucial to understanding the incorporation and preservation of REEs in the fossilized fish teeth. To assess both primary depositional and burial redox conditions, we utilize major and trace element data from the sediments of Core U1356A-98R.

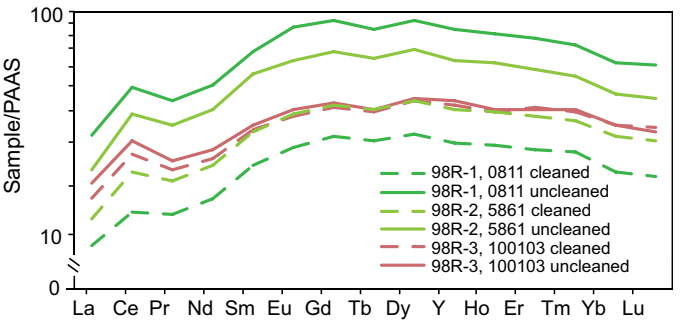

Figure 7. REE profiles of cleaned and uncleaned fossil fish tooth samples normalized to PAAS [*Taylor and McLennan*, 1985].

Redox conditions within sediments and pore waters evolve at depth within the sediment column through a series of oxidant zones.

In areas with oxygenated bottom water, oxygen is available in the upper few to tens of centimeters of the sediment column (oxic zone), but, once consumed, sequential utilization of available oxidants proceeds through the zones in order of highest free energy gain from nitrate and Mn-oxides, Fe-oxides, sulphate, and methane [e.g., *Canfield and Thamdrup*, 2009; *Claypool and Kaplan*, 1974; *Froelich et al*., 1979; *Scott and Lyons*, 2012; *Wang and Van Cappellen*, 1996]. Nitrate reduction forms part of the suboxic zone overlapping with Mn and Fe reduction, and occupies a limited window in the redox process due to the low levels of dissolved nitrate available in seawater. Reduced species produced by the decomposition of organic matter in these suboxic regimes include Mn^{2+}, Fe^{2+}, and NH^{4+}. In sediments containing sufficient organic carbon to drive further redox reactions, the suboxic zone proceeds to sulphate reduction at depth (euxinic zone). A high level of anoxia is present within this zone, where reduction of SO_4^{2-} produces H_2S. The final reaction in redox zones is methanogenesis, which utilizes CO_2 to produce CH_4. Importantly, locations of high sedimentation rates such as continental shelves, can experience suboxic to methanogenic pore water conditions due to rapid burial and oxidation of organic carbon at depth while still having an overlying oxygenated water column [e.g., *Piper and Calvert*, 2009]. For our study, we use the term "anoxic" to encapsulate the oxidant zones that do not consume oxygen (e.g., suboxic, euxinic, methanogenic).

The green mudstone and red claystone sediment layers within Core U1356A-98R are associated with changes in magnetic susceptibility as well as changes in XRF Fe/Rb ratios. Higher magnetic susceptibility, higher Fe concentrations (6–10 wt. %; Figure 2), and increased Fe/Rb ratios are recorded in the red layers, indicating enrichment of ferrimagnetic Fe-oxides such as magnetite. Iron is an extremely redox sensitive element, which is precipitated in sediments under oxic pore water conditions and easily reduced in suboxic pore water conditions, leading to Fe-depletion in the surrounding sediments [e.g., *Anderson and Raiswell*, 2004; *Barnes and Cochran*, 1990; *Klinkhammer et al*., 1982; *Mangini et al*., 2001]. Decreased Fe/Rb ratios and lower magnetic susceptibility within Core U1356A-98R reflect a lower abundance of ferrimagnetic minerals. Low concentrations of Fe (3–5 wt.%; Figure 2) in the green horizons of Core U1356A-98R are therefore indicative of suboxic conditions. This interpretation is supported by an anticorrelation of U and Fe concentrations downcore (Figure 3; supporting information Figure S1; $r^2 = 0.7$). Uranium enrichment in sediments occurs under suboxic and euxinic pore water conditions where the highly soluble U (VI) is reduced to U (IV) and precipitated from pore waters [e.g., *Klinkhammer and Palmer*, 1991]. Uranium concentrations of up to 6 ppm dominate within green layers of Core U1356A-98R and indicate authigenic enrichment (average upper crust abundance = 2.8 ppm) [*McLennan*, 2001].

The variation of Fe and U in the green layers of Core U1356A-98R suggests conditions reached at least a suboxic level. However, we use additional redox sensitive elements to assess the severity of anoxia within these intervals (Figure 3). A key observation is the increase in S/Ti XRF ratios within green layers, likely indicative of changing concentrations of pyrite (Figure 3). This identifies the presence of euxinic conditions within the green layers, as S does not precipitate under suboxic conditions [e.g., *Piper and Calvert*, 2009; *Tribovillard et al*., 2006]. A further suite of elements, Zn, Co, and Cu, also show enrichment within the green intervals (Figure 3). Notably, all of these elements form either their own sulphide species or are incorporated into pyrite, again suggesting an euxinic environment. However, the lack of enrichment of elements such as molybdenum (Mo), which is only fixed under seafloor euxinia [e.g., *Piper and Calvert*, 2009], indicates that these euxinic conditions were probably a product of post burial organic matter decay deeper in the sediment column [e.g., *Algeo and Tribovillard*, 2009]. Therefore, green sediment layers are probably representative of suboxic to euxinic pore water conditions, while red sediment layers were oxic.

5.3. Remobilization of Redox-Sensitive Elements During Diagenesis

Secondary processes such as post depositional reoxygenation may complicate reconstructions of paleoredox signals in sediments. For instance, reoxygenation is known to occur in turbidite sequences due to remobilization of sediments and differential oxygenation during redeposition [e.g., *Chaillou et al*., 2008; *Morford et al*., 2009; *Thomson et al*., 1998]. Such observations may be relevant to our study of Core U1356A-98R due to the sedimentary evidence for gravity flows. Elements such as U are highly susceptible to reoxidation during sediment transport, whereas others such as Cu, Co, and Zn are more robust [e.g., *Thomson et al*., 1998]. Using a suite of trace elements such as these can help to distinguish between primary and secondary redox signals by comparing relative distributions of more- or less-mobile elements.

The green layers of Core U1356A-98R contain evidence, such as the presence of pyrite, for strongly reducing conditions (Figure 3), which may have developed from either (i) deposition under oxygenated bottom water conditions and post burial organic matter oxidation (oxic/suboxic boundary lies at or below sediment-seawater interface) or (ii) deposition under suboxic/anoxic water column (oxic/suboxic boundary lies above sediment-seawater interface). High levels of organic matter burial can drive an increasingly more anoxic sediment environment during sediment burial, even when overlying water column conditions were oxygenated. Conversely, anoxic conditions in the overlying seawater will produce anoxic sediments regardless of organic carbon content. Copper is considered a marker for organic matter fluxes to sediments as it is scavenged by settling organic particles [e.g., *Tribovillard et al*., 2006]. Therefore, we use Cu concentrations as a tracer for increased organic matter content of our sediment samples. The enrichment of Cu in the green layers of Core U1356A-98R suggests that organic matter was/is present in these sediments (Figure 3). Therefore, anoxia likely developed due to organic matter degradation at depth. The presence of organic material in the green layers is further supported by sporomorph data from this core. Green layers of Core U1356A-98R have concentrations of up to 360 pollen spores/g; whereas red layers are completely barren [*Pross et al*., 2012]. The finer-grained red layers of Core U1356A-98R contain higher concentrations of fish teeth (up to 630 teeth/g) suggesting that the red intervals accumulated slowly, allowing complete oxidation under an oxygenated water column.

Based on sediment geochemistry and grain size data, pollen data, and fish tooth accumulation, we interpret alternating oxic and anoxic conditions within the red and green sediments beds of Core U1356A-98R. The green layers most likely represent remobilized shelf sediments containing relatively high levels of organic matter, which were rapidly deposited by sediment gravity flows at Site U1356. These coarser sediments were not oxidized during rapid, shallow burial, and the redox state proceeded to euxinic pore water conditions during further burial as organic matter decayed, evidenced by the formation of pyrite. In contrast, the red layers most likely represent primary oxic deposition of fine-grained material at the seafloor during periods of lower sedimentation rates. Fine-grained sediment particles accumulated in an oxygenated water column, and little or no organic matter was incorporated into these beds. Consequently low organic carbon content and low porosity of the red layers allowed precipitated Fe oxides to remain intact upon burial, preserving an original depositional redox signal.

6. Evaluation of the Integrity of the Nd Isotope Signal in Fossil Fish Teeth

6.1. Source of REEs to Fish Teeth at Site U1356

The terrigenous nature of Site U1356 sediments deposited on the Antarctic continental margin raises a number of concerns for the use of the Nd isotopic composition of fossil fish teeth as a seawater proxy at this site. First, changing redox conditions may influence pore water chemistry, for example, by remobilizing REEs in authigenic coatings. In proximal locations such as Site U1356, there is the potential for these coatings to carry a strong "local" source signature that differs compositionally to ambient seawater (e.g., preformed riverine coatings) [*Bayon et al*., 2004]. REEs released from these phases may affect the REE composition of pore waters and therefore the Nd isotopes recorded in fossil fish teeth. Another potential mechanism for altering REE concentrations is dissolution of in situ sediments (hereafter referred to as sediment flux) [e.g., *Abbott et al*., 2015; *Rousseau et al*., 2015; *Schacht et al*., 2010]. Alternatively, proximity to continental source regions (i.e., dissolved and particulate riverine run-off), as well as exchange processes of pore waters with ambient sediment (i.e., boundary exchange), could shift the authigenic signal towards that of local inputs. Alteration of the Nd isotopic composition of local bottom waters in such scenarios may relay useful information about local/regional processes but can render interpretations on larger-scale ocean circulation difficult [e.g., *Carter et al*., 2012; *Jeandel and Oelkers*, 2015; *Lacan and Jeandel*, 2005; *Pearce et al*., 2013; *Stichel et al*., 2012].

REE profiles extracted from fossil fish tooth and bulk sediment samples from Core U1356A-98R show markedly different patterns and concentrations (Figures 6 and 8) and hence exclude a detrital silicate origin of the fish tooth signal. All fish tooth data from Core U1356A-98R show MREE-enriched "bulge" pattern, along with fish tooth REEs from the Atlantic, Pacific, and Southern Oceans spanning Miocene to Eocene ages, organic matter, FeMn coatings, and a subset of pore water data. While the MREE-enrichment in fossil fish teeth is at least partly controlled by apatite crystal structure and MREE substitution into the Ca^{2+} site

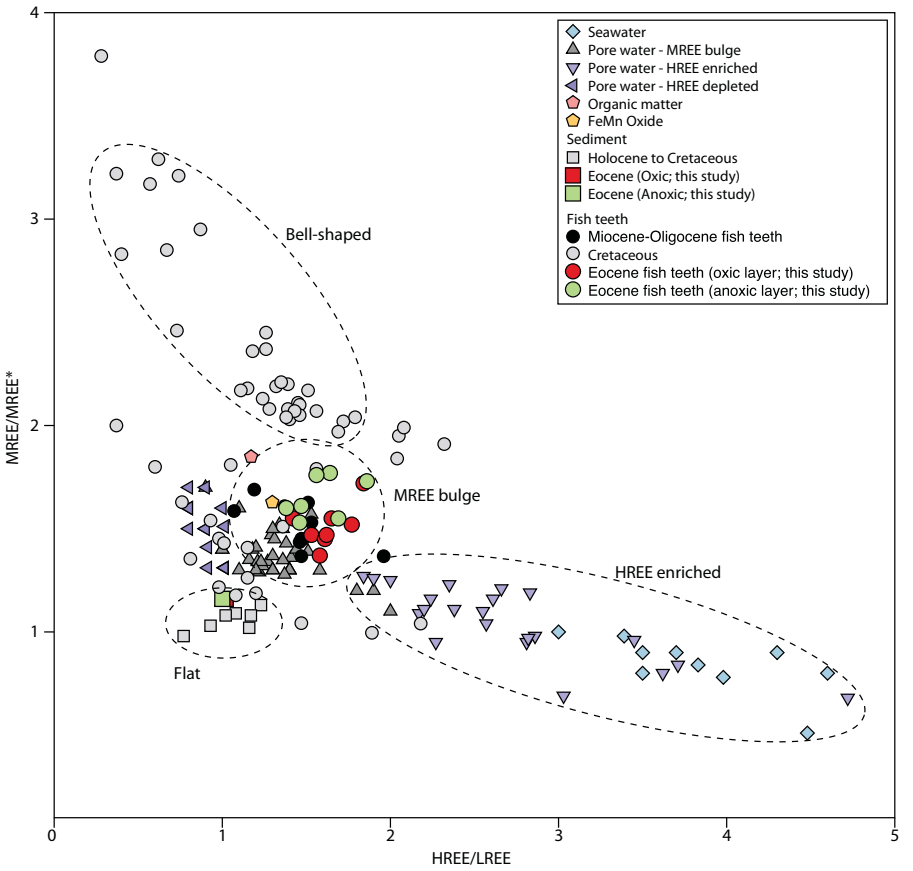

Figure 8. Compilation of non-exhaustive REE data from the literature and this study. HREE/LREE and MREE/MREE* values calculated using method from *Martin et al.* [2010]. HREE: sum of Tm, Yb, and Lu concentrations; LREE: sum of La, Pr, and Nd concentrations; MREE: sum of Gd, Tb, and Dy concentrations; MREE*: (HREE+LREE)/2; all concentrations normalized to PAAS [*Taylor and McLennan*, 1985]. Pore water data: *Abbott et al.* [2015], *Haley et al.* [2004]. Seawater data: *Lacan and Jeandel* [2004] (Atlantic Ocean), *Zhang et al.* [2008] (Indian Ocean), and *Abbott et al.* [2015] (Pacific margin). Organic coating data: *Freslon et al.* [2014]. FeMn oxide data: *Bayon et al.* [2004]. Deep water site fish tooth data: *Martin et al.* [2010] and *Scher et al.* [2011]. Shelf setting fish tooth data: *Charbonnier et al.* [2012], *Moiroud et al.* [2013], and this study. Detrital data: this study, *Gutjahr et al.* [2007], *Charbonnier et al.* [2012], and *Moiroud et al.* [2013]. Dashed circles denote REE pattern groupings with names.

[*Wright et al.*, 1987], the close similarity of the fish tooth REE pattern to MREE-enriched pore water results supports REE provenance from the same source (Figure 8). This source however is distinct from HREE enriched modern seawater and a subset of HREE-enriched pore water analyses, as well as from diagenetically influenced bell-shaped fish tooth REE patterns extracted from Cretaceous shelf sediments [e.g., *Reynard et al.*, 1999] (Figure 8).

Fish tooth REE patterns share the feature of an MREE bulge with FeMn oxyhydroxides and organic matter (Figure 8), both of which could contribute to pore water REE composition upon degradation under anoxic conditions [e.g., *Bayon et al.*, 2011; *Elderfield and Sholkovitz*, 1987; *Haley et al.*, 2004]. *Haley et al.* [2004] reported MREE-enriched patterns for Fe-enriched anoxic pore waters, from continental margin, marine sediments. Recent work on pore water compositions along the Oregon and California margin by *Abbott et al.* [2015], however, has shown that Fe and REE cycling in pore waters is more complex than previously thought, and REE cycling may not be driven by Fe concentrations alone. Fossil fish tooth samples from Core U1356-98R have a consistent MREE-bulge pattern throughout oxic red and anoxic green sediment layers, further supporting the idea that their enriched MREE composition is independent of dissolved Fe concentrations in anoxic sediment pore waters. Furthermore, fish teeth from the green layers lost up to 70% of their REE concentrations during cleaning, while cleaned and uncleaned fish teeth from a red layer show very similar REE concentrations (Figure 7, Table 1). More reducing conditions (in green layers) should yield higher Fe mobility and hence FeMn coatings should be redissolved from the fish tooth surface or present at lower

concentrations. However, we observe the opposite of this, again suggesting that dissolving FeMn coatings (as a source of additional dissolved Fe) are not driving the pore water REE behavior in the sediments at Site U1356.

In contrast to the behavior of FeMn coatings, remineralization of particulate organic matter under anoxic pore water conditions would be consistent with our observations of cleaned and uncleaned fish tooth REE concentrations. Marine particulate organic matter is an important source of authigenic trace metals and REEs to pore waters of continental margins, where it can form organic coatings [e.g., *Freslon et al*., 2014; *Klinkhammer*, 1980; *Sholkovitz et al*., 1994] (Figure 8). Uranium is a good tracer for organometallic compounds [e.g., *McManus et al*., 2006; *Zheng et al*., 2002], and U measurements in cleaned fish tooth samples from green layers (Samples U1356A-98R-1, 8–11 cm and U1356A 98R-2, 58–61 cm) reveal a 70–80% loss in U during cleaning. However, the cleaned and uncleaned pair of fish teeth from a red layer (Sample U1356A-98R-3, 100–103 cm) shows no significant difference in U concentrations. Therefore, organic coatings are likely present on fish teeth extracted from the green layers and are significant carriers of REEs. *Freslon et al*. [2014] have shown that organic coatings are characterized by MREE-enriched, bulge patterns, similar to FeMn oxide/oxyhydroxide coatings and fish teeth (Figures 7 and 8). Overall, our fish tooth REE data suggest that remineralization of sedimentary organic matter under suboxic to anoxic conditions and subsequent formation of organic coatings could have been an important source and process in the cycling of authigenic REEs to the pore waters of Site U1356.

6.2. Fish Tooth Proxy in Shallow Marine Settings: The Ce Anomaly

The one feature of the middle Eocene fish tooth REE patterns from Site U1356 not in agreement with an authigenic origin is their positive Ce anomaly (Figures 6 and 7). Unlike the other REEs, which occur in a trivalent state only, Ce (III) can be oxidized to a highly insoluble tetravalent state (Ce(IV)). Cerium oxidation takes place in shallow water through bacterial mediation [e.g., *Moffett*, 1990] and is typically followed by rapid scavenging/adsorption onto particles (e.g., by FeMn oxyhydroxides), resulting in pronounced negative Ce anomalies in seawater REE patterns (lower Ce concentrations in comparison to neighboring elements Pr and Nd) [e.g., *Alibo and Nozaki*, 1999; *Bau*, 1999; *Tachikawa et al*., 1999]. Negative Ce anomalies have been reported for fish tooth REE patterns from pelagic sites [e.g., *Elderfield and Pagett*, 1986; *Martin et al*., 2010; *Moebius et al*., 2013; *Scher et al*., 2011; *Wright et al*., 1987]. Conversely, positive Ce anomalies in fish teeth have been linked to anoxic seawater conditions [e.g., *Elderfield and Pagett*, 1986; *Wright et al*., 1987]. The fact that we obtained consistently positive Ce anomalies from fish tooth samples throughout both the red (oxic) and green (anoxic) layers (Figure 6) suggests that changing redox conditions of the pore waters at Site U1356 were not the first-order control on the Ce anomaly patterns.

Elderfield and Pagett [1986] demonstrated that FeMn coatings on fish teeth can carry a positive Ce anomaly, while the tooth matrix itself records a negative Ce anomaly. This is not the case for the middle Eocene section at Site U1356, where the cleaned and uncleaned sample pairs reveal the same positive Ce anomaly (Figure 7). Most relevant to our study, positive Ce anomalies in fish teeth have previously been linked to areas of high sedimentation rates, where remineralization of organic matter within the sediment pore waters, leads to anoxic conditions resulting in dissolution of preformed FeMn oxyhydroxides, Ce-oxides and particulate organic matter, and sourcing excess Ce to the pore waters [e.g., *Elderfield and Pagett*, 1986; *Elderfield and Sholkovitz*, 1987; *Freslon et al*., 2014; *Haley et al*., 2004; *Moffett*, 1990; *Sholkovitz et al*., 1992; *Sholkovitz and Elderfield*, 1988]. While such a scenario fits the depositional environment described for the green sediment layers in Core U1356A-98R, it fails to explain similarly positive Ce anomalies in fish teeth extracted from the low sedimentation rate, oxic red layers.

A key factor for the observed positive Ce anomaly may be the proximity of Site U1356 to the continent during the middle Eocene. Cretaceous to Oligocene-aged fish tooth samples from proximal continental margin settings (paleodepths of 200–1500 m) exhibit a consistently positive Ce anomaly [e.g., *Moiroud et al*., 2013; *Scher et al*., 2015]. One simple explanation would be the proximity of Site U1356 to sources of dissolved material from the adjacent continent and the availability of non-scavenged Ce. However, *Rousseau et al*. [2015] have shown that up to 90% of this material is removed from seawater in modern estuaries and does not reach the open ocean. Interestingly, teeth extracted from Site U1356 are amber-to-brown in color, whereas fish teeth from more distal sites, such as Site 757 (Ninety-East Ridge, Indian Ocean), tend to be clear-to-yellow again suggesting a relationship between fish tooth chemistry and a proximal depositional

location. Finally, the similarity of REE patterns in cleaned and uncleaned fish tooth samples could suggest the presence of FeMn oxides or organic phases residing within the internal matrix [e.g., *Tachikawa et al*., 2014]. Further investigation is required to fully understand the relationship between positive fish tooth Ce anomalies and proximal continental margin locations.

6.3. Neodymium Isotopes in Fish Teeth at Site U1356

REE patterns of fish teeth at Site U1356 suggest the preservation of an authigenic signal, but we cannot rule out the possibility of a contribution of REEs from sedimentary fluxes to the pore waters based on interpreting pattern shape alone. The remaining question to address is whether the Nd isotopic composition of fossil fish teeth at Site U1356 during the middle Eocene records ambient seawater or a mixture of seawater and sediment dissolution or continental fluxes. $\varepsilon_{Nd(t)}$ values of fish tooth and bulk sediment samples are consistently offset by ~2.5 ε_{Nd} units in samples from both red and green layers in Core U1356A-98R (Figure 5). This indicates that the fish teeth are indeed recording and preserving a Nd isotopic composition that is dominated by a source different to the sediments (i.e., seawater) and that there is no significant increase in lithogenic-sourced Nd to the fish teeth during oxic or anoxic depositional conditions.

Modern seawater on the shallow (~300 m) Adélie shelf, in close proximity to Site U1356, is characterized by ε_{Nd} values between −9.3 and −10.5 [*Lambelet et al*., 2014]. All our fish tooth values ($\varepsilon_{Nd(t)} = -10.5$ to −12.5) fall between the range of modern seawater results and that of Eocene sediments ($\varepsilon_{Nd(t)} = -14.0$ and −15.1). If a simple isotopic mixing model is applied, this results in a potential sedimentary contribution to the pore waters of up to 40%. However, this model assumes similar Nd concentrations in both end-members. This is unjustified for sediments, which carry Nd concentrations that are several orders of magnitude higher than typical seawater. Thus very small amounts of sediment dissolution could potentially affect the pore water Nd isotopic composition recorded by the fish teeth. *Abbott et al*. [2015] showed that the pore waters of continental margins carry Nd concentrations at least one order of magnitude higher than ambient seawater. In our case, seawater and sediment end-member constraints ($[Nd]_{seawater} = \sim 3$ ng/kg, $\varepsilon_{Nd\ seawater} \sim -10$; average $[Nd]_{sediment} = 30.4$ ppm, average $\varepsilon_{Nd(t)\ sediment} = -14.3$) suggest that sediment dissolution of about 0.0000001% is all that is needed to shift the Nd isotopic composition of pore waters from a seawater value (and concentration) to the lowest observed Nd isotopic composition of −12.5. The resulting pore water Nd concentration would be elevated from seawater by a factor of ~4. While within the range of published pore water concentrations [e.g., *Haley et al*., 2004], *Abbott et al*. [2015] indicate that this maximum pore waters REE enrichment occurs at a depth of ~5–10 cm in the sediment column. At this level, fish teeth may have already fossilized [e.g., *Bernat*, 1975; *Elderfield and Pagett*, 1986; *Martin and Haley*, 2000; *Reynard et al*., 1999; *Sholkovitz et al*., 1989; *Staudigel et al*., 1985] recording an authigenic signal unaffected by sediment fluxes. Diffusion of REE (sourced from sediment dissolution) through the sediment column is most effective for MREEs, while HREEs and LREEs (including Nd) are preferentially readsorbed or complexed [*Abbott et al*., 2015]. Thus sediment-sourced Nd may be rapidly readsorbed in the vicinity of its dissolving parent material. Overall, we conclude that a major imprint of Nd sourced from dissolving sediment, on the signature recorded by the fish teeth from Core U1356-98R is unlikely.

Our study highlights questions regarding the robustness of different archive phases, routinely used in paleoceanographic studies. Future combined studies of pore waters, sediments, fish teeth, and ambient seawater, ideally showing transitions between oxic and anoxic conditions, will be needed to reveal the exact mass balance and the processes involved in generating the composition of REEs preserved by fish teeth, and other archives, in shallow marine, source-proximal settings. It is worth noting that whether the Nd isotopic composition of pore waters in the shallow marine setting of Site U1356 was set by sedimentary flux, or direct continental run-off, this could still be the signature exported in bottom waters to other regions within the water mass. A suitable analogue here is today's Adélie Land Bottom Water, which acquires its signature on the Antarctic shelf, but is then exported as Antarctic Bottom Water [*Lambelet et al*., 2014; *van de Flierdt et al*., 2006]. Caution is hence justified when using Nd isotopic compositions of fish teeth from shallow marine sites for unraveling the history of water mass mixing.

7. Conclusions

Sediments from a mid-Eocene shallow marine section at IODP Site U1356 off East Antarctica were deposited under redox conditions varying between oxic and anoxic and at changing depositional rates. Alternating

redox conditions within the sedimentary layers are identified by a range of major and trace elements. REE concentrations and Nd isotopic compositions of fossil fish teeth do not covary with these same layers, suggesting that the Nd isotopic composition preserved by fossil fish teeth was not affected by these changing redox conditions. Mid-REE enriched patterns, combined with elevated U levels in uncleaned fish teeth from green (anoxic) layers, suggest that fish teeth acquired their Nd isotope signatures from the sediment pore waters during early diagenesis. The pore waters in turn were influenced by remineralization of organic matter carrying an authigenic signature. Organic matter-derived coatings on fish tooth samples from green layers, contained up to 70% of the total REE concentration of the fish tooth and may represent a significant archive of authigenic REEs. Persistently positive Ce anomalies in fish teeth, regardless of the oxygenation levels of the host sediments, however indicate that the shallow marine setting of Site U1356 in the middle Eocene may have been influenced by dissolved continental inputs. The reconstructed seawater Nd isotopic compositions from fossil fish teeth at Site U1356 are consistent with modern seawater data, but will have to be interpreted in the context of a longer record.

Acknowledgments

This manuscript benefited from the insightful reviews of Marcus Gutjahr and one anonymous reviewer. We thank B. Coles, K. Kreissig (Imperial College), and V. Lukies (MARUM) for technical laboratory support. We acknowledge the Expedition 318 Scientists for producing the shipboard data used in this study. This research used samples and data provided by IODP. Funding for this research was provided by a NERC UK IODP grant awarded to T.vd.F. and S.M.B. (NE/I006257/1), an ECORD Research grant awarded to C.E.H., and DFG grant (RO 113/6) to U.R. F.J.J.E. acknowledges financial support from MEXT-Japan and the Spanish Ministry of Science and Innovation grant CTM 2011-24079. All data used for this study are available from the Tables, cited references, supporting information and on the Pangaea database (www.pangaea.de). The authors declare no conflicting interests.

References

Abbott, A. N., B. A. Haley, J. McManus, and C. E. Reimers (2015), The sedimentary flux of dissolved rare earth elements to the ocean, *Geochim. Cosmochim. Acta*, *154*, 186–200.

Algeo, T., and N. Tribovillard (2009), Environmental analysis of paleoceanographic systems based on molybdenum–uranium covariation, *Chem. Geol.*, *268*(3), 211–225.

Alibo, D. S., and Y. Nozaki (1999), Rare earth elements in seawater: Particle association, shale-normalization, and Ce oxidation, *Geochim. Cosmochim. Acta*, *63*(3), 363–372.

Anderson, T. F., and R. Raiswell (2004), Sources and mechanisms for the enrichment of highly reactive iron in euxinic Black Sea sediments, *Am. J. Sci.*, *304*(3), 203–233.

Arrhenius, G., M. N. Bramlette, and E. Picciotto (1957), Localization of radioactive and stable heavy nuclides in ocean sediments, *Nature*, *180*(4576), 85–86.

Barnes, C. E., and J. K. Cochran (1990), Uranium removal in oceanic sediments and the oceanic U balance, *Earth Planet. Sci. Lett.*, *97*(1–2), 94–101.

Bau, M. (1999), Scavenging of dissolved yttrium and rare earths by precipitating iron oxyhydroxide: Experimental evidence for Ce oxidation, Y-Ho fractionation, and lanthanide tetrad effect, *Geochim. Cosmochim. Acta*, *63*(1), 67–77.

Bau, M., A. Koschinsky, P. Dulski, and J. R. Hein (1996), Comparison of the partitioning behaviours of yttrium, rare earth elements, and titanium between hydrogenetic marine ferromanganese crusts and seawater, *Geochim. Cosmochim. Acta*, *60*(10), 1709–1725.

Bau, M., P. Möller, and P. Dulski (1997), Yttrium and lanthanides in eastern Mediterranean seawater and their fractionation during redox-cycling, *Mar. Chem.*, *56*(1–2), 123–131.

Bayon, G., C. German, R. Boella, J. Milton, R. Taylor, and R. Nesbitt (2002), An improved method for extracting marine sediment fractions and its application to Sr and Nd isotopic analysis, *Chem. Geol.*, *187*(3), 179–199.

Bayon, G., C. R. German, K. W. Burton, R. W. Nesbitt, and N. Rogers (2004), Sedimentary Fe–Mn oxyhydroxides as paleoceanographic archives and the role of aeolian flux in regulating oceanic dissolved REE, *Earth Planet. Sci. Lett.*, *224*(3–4), 477–492.

Bayon, G., D. Birot, L. Ruffine, J.-C. Caprais, E. Ponzevera, C. Bollinger, J.-P. Donval, J.-L. Charlou, M. Voisset, and S. Grimaud (2011), Evidence for intense REE scavenging at cold seeps from the Niger Delta margin, *Earth Planet. Sci. Lett.*, *312*(3), 443–452.

Bea, F., P. Montero, A. Stroh, and J. Baasner (1996), Microanalysis of minerals by an Excimer UV-LA-ICP-MS system, *Chem. Geol.*, *133*(1), 145–156.

Bernat, M. (1975), Les isotopes de l'uranium et du thorium et les terres rares dans l'environnement marin, *Cah. ORSTOM Ser. Geol.*, *7*, 65–83.

Bijl, P. K., J. A. Bendle, S. M. Bohaty, J. Pross, S. Schouten, L. Tauxe, C. E. Stickley, R. M. McKay, U. Röhl, and M. Olney (2013), Eocene cooling linked to early flow across the Tasmanian Gateway, *Proc. Natl. Acad. Sci. U. S. A.*, *110*(24), 9645–9650.

Borg, S. G., and D. J. DePaolo (1991), A tectonic model of the Antarctic Gondwana margin with implications for southeastern Australia: Isotopic and geochemical evidence, *Tectonophysics*, *196*(3), 339–358.

Boyle, E. A., and L. Keigwin (1987), North Atlantic thermohaline circulation during the past 20,000 years linked to high-latitude surface temperature, *Nature*, *330*(6143), 35–40.

Canfield, D., and B. Thamdrup (2009), Towards a consistent classification scheme for geochemical environments, or, why we wish the term 'suboxic'would go away, *Geobiology*, *7*(4), 385–392.

Carter, P., D. Vance, C. Hillenbrand, J. Smith, and D. Shoosmith (2012), The neodymium isotopic composition of waters masses in the eastern Pacific sector of the Southern Ocean, *Geochim. Cosmochim. Acta*, *79*, 41–59.

Chaillou, G., J. Schäfer, G. Blanc, and P. Anschutz (2008), Mobility of Mo, U, As, and Sb within modern turbidites, *Mar. Geol.*, *254*(3–4), 171–179.

Charbonnier, G., et al. (2012), Reconstruction of the Nd isotope composition of seawater on epicontinental seas: Testing the potential of Fe–Mn oxyhydroxide coatings on foraminifera tests for deep-time investigations, *Geochim. Cosmochim. Acta*, *99*(0), 39–56.

Chavagnac, V., J. Milton, D. Green, J. Breuer, O. Bruguier, D. Jacob, T. Jong, G. Kamenov, J. Le Huray, and Y. Liu (2007), Towards the development of a fossil bone geochemical standard: An inter-laboratory study, *Anal. Chim. Acta*, *599*(2), 177–190.

Claypool, G. E., and I. Kaplan (1974), The origin and distribution of methane in marine sediments, in *Natural Gases in Marine Sediments*, edited by Isaac R. Kaplan, pp. 99–139, Springer, U.S.

Close, D. I., A. B. Watts, and H. M. J. Stagg (2009), A marine geophysical study of the Wilkes Land rifted continental margin, Antarctica, *Geophys. J. Int.*, *177*(2), 430–450.

De Baar, H. J., M. P. Bacon, P. G. Brewer, and K. W. Bruland (1985), Rare earth elements in the Pacific and Atlantic Oceans, *Geochim. Cosmochim. Acta*, *49*(9), 1943–1959.

Elderfield, H., and R. Pagett (1986), Rare earth elements in ichthyoliths: Variations with redox conditions and depositional environment, *Sci. Total Environ.*, *49*, 175–197.

Elderfield, H., and E. T. Sholkovitz (1987), Rare earth elements in the pore waters of reducing nearshore sediments, *Earth Planet. Sci. Lett.*, *82*(3), 280–288.
Escutia, C., H. Brinkhaus, A. Klaus (2011), and the Expedition 318 Scientists Proceedings of the IODP, Volume 318 (Integrated Ocean Drilling Program Management International, Inc., Tokyo).
Frank, M. (2002), Radiogenic isotopes: Tracers of past ocean circulation and erosional input, *Rev. Geophys.*, *40*(1), 1001, doi:10.1029/2000RG000094.
Freslon, N., G. Bayon, S. Toucanne, S. Bermell, C. Bollinger, S. Chéron, J. Etoubleau, Y. Germain, A. Khripounoff, and E. Ponzevera (2014), Rare earth elements and neodymium isotopes in sedimentary organic matter, *Geochim. Cosmochim. Acta*, *140*, 177–198.
Froelich, P., G. Klinkhammer, M. A. A. Bender, N. Luedtke, G. R. Heath, D. Cullen, P. Dauphin, D. Hammond, B. Hartman, and V. Maynard (1979), Early oxidation of organic matter in pelagic sediments of the eastern equatorial Atlantic: Suboxic diagenesis, *Geochim. Cosmochim. Acta*, *43*(7), 1075–1090.
Garcia-Solsona, E., C. Jeandel, M. Labatut, F. Lacan, D. Vance, V. Chavagnac, and C. Pradoux (2014), Rare earth elements and Nd isotopes tracing water mass mixing and particle-seawater interactions in the SE Atlantic, *Geochim. Cosmochim. Acta*, *125*, 351–372.
Giosan, L., R. D. Flood, and R. C. Aller (2002), Paleoceanographic significance of sediment color on western North Atlantic drifts: I. Origin of color, *Mar. Geol.*, *189*(1), 25–41.
Goldstein, S. J., and S. B. Jacobsen (1987), The Nd and Sr isotopic systematics of river-water dissolved material: Implications for the sources of Nd and Sr in seawater, *Chem. Geol.*, *66*(3), 245–272.
Goldstein, S. L., and S. R. Hemming (2003), Long-lived isotopic tracers in oceanography, paleoceanography, and ice-sheet dynamics, *Treat. Geochem.*, *6*, 453–489.
Govindaraju, K. (1994), Compilation of working values and sample description for 383 geostandards, *Geostand. Newsl.*, *18*, 1–158.
Gutjahr, M., M. Frank, C. H. Stirling, V. Klemm, T. van de Flierdt, and A. N. Halliday (2007), Reliable extraction of a deepwater trace metal isotope signal from Fe-Mn oxyhydroxide coatings of marine sediments, *Chem. Geol.*, *242*(3-4), 351–370.
Haley, B. A., G. P. Klinkhammer, and J. McManus (2004), Rare earth elements in pore waters of marine sediments, *Geochim. Cosmochim. Acta*, *68*(6), 1265–1279.
Jacobsen, S. B., and G. Wasserburg (1980), Sm-Nd isotopic evolution of chondrites, *Earth Planet. Sci. Lett.*, *50*(1), 139–155.
Jeandel, C., and E. H. Oelkers (2015), The influence of terrigenous particulate material dissolution on ocean chemistry and global element cycles, *Chem. Geol.*, *395*, 50–66.
Jeandel, C., T. Arsouze, F. Lacan, P. Techine, and J.-C. Dutay (2007), Isotopic Nd compositions and concentrations of the lithogenic inputs into the ocean: A compilation, with an emphasis on the margins, *Chem. Geol.*, *239*(1), 156–164.
Klinkhammer, G., D. T. Heggie, and D. W. Graham (1982), Metal diagenesis in oxic marine sediments, *Earth Planet. Sci. Lett.*, *61*(2), 211–219.
Klinkhammer, G. P. (1980), Early diagenesis in sediments from the eastern equatorial Pacific, II. Pore water metal results, *Earth Planet. Sci. Lett.*, *49*(1), 81–101.
Klinkhammer, G. P., and M. R. Palmer (1991), Uranium in the oceans: Where it goes and why, *Geochim. Cosmochim. Acta*, *55*(7), 1799–1806.
Kocsis, L., C. N. Trueman, and M. R. Palmer (2010), Protracted diagenetic alteration of REE contents in fossil bioapatites: Direct evidence from Lu–Hf isotope systematics, *Geochim. Cosmochim. Acta*, *74*(21), 6077–6092.
Lacan, F., and C. Jeandel (2004), Neodymium isotopic composition and rare earth element concentrations in the deep and intermediate Nordic Seas: Constraints on the Iceland Scotland Overflow Water signature, *Geochem. Geophys. Geosyst.*, *5*, doi:10.1029/2004GC000742.
Lacan, F., and C. Jeandel (2005), Neodymium isotopes as a new tool for quantifying exchange fluxes at the continent-ocean interface, *Earth Planet. Sci. Lett.*, *232*(3), 245–257.
Lacan, F., K. Tachikawa, and C. Jeandel (2012), Neodymium isotopic composition of the oceans: A compilation of seawater data, *Chem. Geol.*, *300*, 177–184.
Lambelet, M., T. van de Flierdt, E.C. V. Butler, A. R. Bowie, S. R. Rintoul, R. J. Watson, T. Remenyl, and D. Lannuzel (2014), The Nd isotopic compositions of Adélie Coast Bottom Water: Insights from GIPY6 Cruise along 140', Abstract #OS21G-07 presented at 2014 Fall Meeting 2014, AGU, San Francisco, Calif.
MacLeod, K. G., E. E. Martin, and S. W. Blair (2008), Nd isotopic excursion across Cretaceous ocean anoxic event 2 (Cenomanian-Turonian) in the tropical North Atlantic, *Geology*, *36*(10), 811–814.
MacLeod, K. G., C. I. Londoño, E. Martin, Á. J. Berrocoso, and C. Basak (2011), Changes in North Atlantic circulation at the end of the Cretaceous greenhouse interval, *Nat. Geosci.*, *4*(11), 779–782.
Mangini, A., M. Jung, and S. Laukenmann (2001), What do we learn from peaks of uranium and of manganese in deep sea sediments?, *Mar. Geol.*, *177*(1), 63–78.
Martin, E. E., and B. A. Haley (2000), Fossil fish teeth as proxies for seawater Sr and Nd isotopes, *Geochim. Cosmochim. Acta*, *64*(5), 835–847.
Martin, E. E., and H. D. Scher (2004), Preservation of seawater Sr and Nd isotopes in fossil fish teeth: Bad news and good news, *Earth Planet. Sci. Lett.*, *220*(1-2), 25–39.
Martin, E. E., and H. D. Scher (2006), A Nd isotopic study of southern sourced waters and Indonesian throughflow at intermediate depths in the Cenozoic Indian Ocean, *Geochem. Geophy. Geosyst.*, *7*, Q09N02, doi:10.1029/2006GC001302.
Martin, E. E., S. W. Blair, G. D. Kamenov, H. D. Scher, E. Bourbon, C. Basak, and D. N. Newkirk (2010), Extraction of Nd isotopes from bulk deep sea sediments for paleoceanographic studies on Cenozoic time scales, *Chem. Geol.*, *269*(3), 414–431.
Martin, E. E., K. MacLeod, A. Jiménez Berrocoso, and E. Bourbon (2012), Water mass circulation on Demerara Rise during the Late Cretaceous based on Nd isotopes, *Earth Planet. Sci. Lett.*, *327*, 111–120.
McLennan, S. M. (2001), Relationships between the trace element composition of sedimentary rocks and upper continental crust, *Geochem. Geophys. Geosyst.*, *2*(4), 1021.
McManus, J., W. M. Berelson, S. Severmann, R. L. Poulson, D. E. Hammond, G. P. Klinkhammer, and C. Holm (2006), Molybdenum and uranium geochemistry in continental margin sediments: Paleoproxy potential, *Geochim. Cosmochim. Acta*, *70*(18), 4643–4662.
Moebius, I., O. Friedrich, K. Edgar, H. Scher, and P. Sexton (2013), Bottom water changes in the subtropical North Atlantic and the Southern Ocean associated to the Middle Eocene Climatic Optimum, Abstract PP31A-1852 presented at 2013 Fall Meeting, AGU, San Francisco, Calif.
Moffett, J. W. (1990), Microbially mediated cerium oxidation in sea water, *Nature*, *345*, 421–423.
Moiroud, M., E. Pucéat, Y. Donnadieu, G. Bayon, K. Moriya, J.-F. Deconinck, and M. Boyet (2013), Evolution of the neodymium isotopic signature of neritic seawater on a northwestern Pacific margin: New constrains on possible end-members for the composition of deep-water masses in the Late Cretaceous ocean, *Chem. Geol.*, *356*, 160–170.
Morford, J. L., W. R. Martin, and C. M. Carney (2009), Uranium diagenesis in sediments underlying bottom waters with high oxygen content, *Geochim. Cosmochim. Acta*, *73*(10), 2920–2937.

Pearce, C. R., M. T. Jones, E. H. Oelkers, C. Pradoux, and C. Jeandel (2013), The effect of particulate dissolution on the neodymium (Nd) isotope and Rare Earth Element (REE) composition of seawater, *Earth Planet. Sci. Lett.*, *369*, 138–147.
Pin, C., and J. S. Zalduegui (1997), Sequential separation of light rare-earth elements, thorium and uranium by miniaturized extraction chromatography: Application to isotopic analyses of silicate rocks, *Anal. Chim. Acta*, *339*(1), 79–89.
Piper, D., and S. Calvert (2009), A marine biogeochemical perspective on black shale deposition, *Earth Sci. Rev.*, *95*(1), 63–96.
Potter, P. E., J. B. Maynard, and P. J. Depetris (2005), Mud and mudstones: Introduction and overview, Springer Science & Business Media, Berlin, Heidelberg.
Pross, J., L. Contreras, P. K. Bijl, D. R. Greenwood, S. M. Bohaty, S. Schouten, J. A. Bendle, U. Röhl, L. Tauxe, and J. I. Raine (2012), Persistent near-tropical warmth on the Antarctic continent during the early Eocene epoch, *Nature*, *488*(7409), 73–77.
Pucéat, E., C. Lécuyer, and L. Reisberg (2005), Neodymium isotope evolution of NW Tethyan upper ocean waters throughout the Cretaceous, *Earth Planet. Sci. Lett.*, *236*(3), 705–720.
Reynard, B., C. Lécuyer, and P. Grandjean (1999), Crystal-chemical controls on rare-earth element concentrations in fossil biogenic apatites and implications for paleoenvironmental reconstructions, *Chem. Geol.*, *155*(3–4), 233–241.
Roberts, N. L., A. M. Piotrowski, J. F. McManus, and L. D. Keigwin (2010), Synchronous deglacial overturning and water mass source changes, *Science*, *327*(5961), 75–78.
Robinson, S. A., and D. Vance (2012), Widespread and synchronous change in deep-ocean circulation in the North and South Atlantic during the Late Cretaceous, *Paleoceanography*, *27*, PA1102, doi:10.1029/2011PA002240.
Robinson, S. A., D. P. Murphy, D. Vance, and D. J. Thomas (2010), Formation of "Southern Component Water" in the late cretaceous: Evidence from Nd-isotopes, *Geology*, *38*(10), 871–874.
Rousseau, T. C. C. et al. (2015), Rapid neodymium release to marine waters from lithogenic sediments in the Amazon estuary, *Nat. Commun.*, *6*, 7592, doi:10.1038/ncomms8592.
Rutberg, R. L., S. R. Hemming, and S. L. Goldstein (2000), Reduced North Atlantic Deep Water flux to the glacial Southern Ocean inferred from neodymium isotope ratios, *Nature*, *405*(6789), 935–938.
Schacht, U., K. Wallmann, and S. Kutterolf (2010), The influence of volcanic ash alteration on the REE composition of marine pore waters, *J. Geochem. Explor.*, *106*(1), 176–187.
Scher, H. D., and M. L. Delaney (2010), Breaking the glass ceiling for high resolution Nd isotope records in early Cenozoic paleoceanography, *Chem. Geol.*, *269*(3), 329–338.
Scher, H. D., and E. E. Martin (2004), Circulation in the Southern Ocean during the Paleogene inferred from neodymium isotopes, *Earth Planet. Sci. Lett.*, *228*(3-4), 391–405.
Scher, H. D., and E. E. Martin (2008), Oligocene deep water export from the North Atlantic and the development of the Antarctic Circumpolar Current examined with neodymium isotopes, *Paleoceanography*, *23*, PA1205, doi:10.1029/2006PA001400.
Scher, H. D., S. M. Bohaty, J. C. Zachos, and M. L. Delaney (2011), Two-stepping into the icehouse: East Antarctic weathering during progressive ice-sheet expansion at the Eocene–Oligocene transition, *Geology*, *39*(4), 383–386.
Scher, H. D., J. M. Whittaker, S. E. Williams, J. C. Latimer, W. E. Kordesch, and M. L. Delaney (2015), Onset of Antarctic Circumpolar Current 30 million years ago as Tasmanian Gateway aligned with westerlies, *Nature*, *523*(7562), 580–583.
Scott, C., and T. W. Lyons (2012), Contrasting molybdenum cycling and isotopic properties in euxinic versus non-euxinic sediments and sedimentary rocks: Refining the paleoproxies, *Chem. Geol.*, *324–325*, 19–27.
Shaw, H., and G. Wasserburg (1985), Sm-Nd in marine carbonates and phosphates: Implications for Nd isotopes in seawater and crustal ages, *Geochim. Cosmochim. Acta*, *49*(2), 503–518.
Sholkovitz, E. R., and H. Elderfield (1988), Cycling of dissolved rare earth elements in Chesapeake Bay, *Global Biogeochem. Cycles*, *2*(2), 157–176.
Sholkovitz, E. R., D. J. Piepgras, and S. B. Jacobsen (1989), The pore water chemistry of rare earth elements in Buzzards Bay sediments, *Geochim. Cosmochim. Acta*, *53*(11), 2847–2856.
Sholkovitz, E. R., T. J. Shaw, and D. Schneider (1992), The geochemistry of rare earth elements in the seasonally anoxic water column and porewaters of Chesapeake Bay, *Geochim. Cosmochim. Acta*, *56*(9), 3389–3402.
Sholkovitz, E. R., W. M. Landing, and B. L. Lewis (1994), Ocean particle chemistry: The fractionation of rare earth elements between suspended particles and seawater, *Geochim. Cosmochim. Acta*, *58*(6), 1567–1579.
Staudigel, H., P. Doyle, and A. Zindler (1985), Sr and Nd isotope systematics in fish teeth, *Earth Planet. Sci. Lett.*, *76*(1), 45–56.
Stichel, T., M. Frank, J. Rickli, E. C. Hathorne, B. A. Haley, C. Jeandel, and C. Pradoux (2012), Sources and input mechanisms of hafnium and neodymium in surface waters of the Atlantic sector of the Southern Ocean, *Geochim. Cosmochim. Acta*, *94*, 22–37.
Tachikawa, K., C. Jeandel, A. Vangriesheim, and B. Dupré (1999), Distribution of rare earth elements and neodymium isotopes in suspended particles of the tropical Atlantic Ocean (EUMELI site), *Deep Sea Res., Part I*, *46*(5), 733–755.
Tachikawa, K., V. Athias, and C. Jeandel (2003), Neodymium budget in the modern ocean and paleo-oceanographic implications, *J. Geophys. Res.*, *108*(C8), 3254, doi:10.1029/1999JC000285.
Tachikawa, K., A. M. Piotrowski, and G. Bayon (2014), Neodymium associated with foraminiferal carbonate as a recorder of seawater isotopic signatures, *Quat. Sci. Rev.*, *88*, 1–13.
Tanaka, T., S. Togashi, H. Kamioka, H. Amakawa, H. Kagami, T. Hamamoto, M. Yuhara, Y. Orihashi, S. Yoneda, and H. Shimizu (2000), JNdi-1: A neodymium isotopic reference in consistency with LaJolla neodymium, *Chem. Geol.*, *168*(3), 279–281.
Tauxe, L., et al. (2012), Chronostratigraphic framework for the IODP Expedition 318 cores from the Wilkes Land Margin: Constraints for paleoceanographic reconstruction, *Paleoceanography*, *27*, PA2214, doi:10.1029/2012PA002308.
Taylor, S. R., and S. M. McLennan (1985), The continental crust: Its composition and evolution, 312 pp., Blackwell Scientific Publications, Oxford, U. K.
Thomas, D. J., T. J. Bralower, and C. E. Jones (2003), Neodymium isotopic reconstruction of late Paleocene-early Eocene thermohaline circulation, *Earth Planet. Sci. Lett.*, *209*(3-4), 309–322.
Thomas, D. J., M. Lyle, T. C. Moore, and D. K. Rea (2008), Paleogene deepwater mass composition of the tropical Pacific and implications for thermohaline circulation in a greenhouse world, *Geochem. Geophys. Geosyst.*, *9*, Q02002, doi:10.1029/2007GC001748.
Thomas, D. J., R. Korty, M. Huber, J. A. Schubert, and B. Haines (2014), Nd isotopic structure of the Pacific Ocean 70–30 Ma and numerical evidence for vigorous ocean circulation and ocean heat transport in a greenhouse world, *Paleoceanography*, *29*, 454–469, doi:10.1002/2013PA002535.
Thomson, J., I. Jarvis, D. R. Green, D. A. Green, and T. Clayton (1998), Mobility and immobility of redox-sensitive elements in deep-sea turbidites during shallow burial, *Geochim. Cosmochim. Acta*, *62*(4), 643–656.
Tribovillard, N., T. J. Algeo, T. Lyons, and A. Riboulleau (2006), Trace metals as paleoredox and paleoproductivity proxies: An update, *Chem. Geol.*, *232*(1), 12–32.

Turner, S., J. Foden, M. Sandiford, and D. Bruce (1993), Sm-Nd isotopic evidence for the provenance of sediments from the Adelaide Fold Belt and southeastern Australia with implications for episodic crustal addition, *Geochim. Cosmochim. Acta*, *57*(8), 1837–1856.

Tütken, T., and T. W. Vennemann (2011), Fossil bones and teeth: Preservation or alteration of biogenic compositions?, *Palaeogeogr. Palaeoclimatol. Palaeoecol.*, *310*(1–2), 1–8.

van de Flierdt, T., and M. Frank (2010), Neodymium isotopes in paleoceanography-introduction, *Quat. Sci. Rev.*, *29*, 2439–2441.

van de Flierdt, T., S. R. Hemming, S. L. Goldstein, and W. Abouchami (2006), Radiogenic isotope fingerprint of Wilkes Land–Adélie Coast Bottom Water in the circum-Antarctic Ocean, *Geophys. Res. Lett.*, *33*, L12606, doi:10.1029/2006GL026020.

Wang, Y., and P. Van Cappellen (1996), A multicomponent reactive transport model of early diagenesis: Application to redox cycling in coastal marine sediments, *Geochim. Cosmochim. Acta*, *60*(16), 2993–3014.

Weis, D., B. Kieffer, C. Maerschalk, J. Barling, J. de Jong, G. A. Williams, D. Hanano, W. Pretorius, N. Mattielli and J. S. Scoates (2006), High-precision isotopic characterization of USGS reference materials by TIMS and MC-ICP-MS, *Geochem. Geophys. Geosyst.*, *7*, Q08006, doi: 10.1029/2006GC001283.

Wilson, D. J., A. M. Piotrowski, A. Galy, and J. A. Clegg (2013), Reactivity of neodymium carriers in deep sea sediments: Implications for boundary exchange and paleoceanography, *Geochim. Cosmochim. Acta*, *109*, 197–221.

Wilson, D. S., S. S. R. Jamieson, P. J. Barrett, G. Leitchenkov, K. Gohl, and R. D. Larter (2012), Antarctic topography at the Eocene–Oligocene boundary, *Palaeogeogr. Palaeoclimatol. Palaeoecol.*, *335–336*, 24–34.

Wright, J., H. Schrader, and W. T. Holser (1987), Paleoredox variations in ancient oceans recorded by rare earth elements in fossil apatite, *Geochim. Cosmochim. Acta*, *51*(3), 631–644.

Zhang, Y., F. Lacan, and C. Jeandel (2008), Dissolved rare earth elements tracing lithogenic inputs over the Kerguelen Plateau (Southern Ocean), *Deep Sea Res., Part II*, *55*(5), 638–652.

Zheng, Y., R. F. Anderson, A. van Geen, and M. Q. Fleisher (2002), Remobilization of authigenic uranium in marine sediments by bioturbation, *Geochim. Cosmochim. Acta*, *66*(10), 1759–1772.